NeuroImage 255 (2022) 119193

Contents lists available at ScienceDirect

NeuroImage

journal homepage: www.elsevier.com/locate/neuroimage

Discovering hidden brain network responses to naturalistic stimuli via tensor component analysis of multi-subject fMRI data

Guoqiang Hu[a], Huanjie Li[a], Wei Zhao[a], Yuxing Hao[a], Zonglei Bai[b], Lisa D. Nickerson[c,d,*], Fengyu Cong[a,e,f,g,*]

[a] School of Biomedical Engineering, Faculty of Electronic Information and Electrical Engineering, Dalian University of Technology, Dalian, China
[b] School of Electronics Engineering and Computer Science, Peking University, Beijing, China
[c] Brain Imaging Center, Mclean Hospital, Belmont, MA, USA
[d] Department of Psychiatry, Harvard Medical School, Boston, MA, USA
[e] School of Artificial Intelligence, Faculty of Electronic Information and Electrical Engineering, Dalian University of Technology, Dalian, China
[f] Key Laboratory of Integrated Circuit and Biomedical Electronic System, Liaoning Province. Dalian University of Technology, Dalian, China
[g] Faculty of Information Technology, University of Jyvaskyla, Jyvaskyla, Finland

ARTICLE INFO

Keywords:
Tensor components analysis
Naturalistic stimuli
fMRI
Inter-subject correlation

ABSTRACT

The study of brain network interactions during naturalistic stimuli facilitates a deeper understanding of human brain function. To estimate large-scale brain networks evoked with naturalistic stimuli, a tensor component analysis (TCA) based framework was used to characterize shared spatio-temporal patterns across subjects in a purely data-driven manner. In this framework, a third-order tensor is constructed from the timeseries extracted from all brain regions from a given parcellation, for all participants, with modes of the tensor corresponding to spatial distribution, time series and participants. TCA then reveals spatially and temporally shared components, i.e., evoked networks with the naturalistic stimuli, their time courses of activity and subject loadings of each component. To enhance the reproducibility of the estimation with the adaptive TCA algorithm, a novel spectral clustering method, tensor spectral clustering, was proposed and applied to evaluate the stability of the TCA algorithm. We demonstrated the effectiveness of the proposed framework via simulations and real fMRI data collected during a motor task with a traditional fMRI study design. We also applied the proposed framework to fMRI data collected during passive movie watching to illustrate how reproducible brain networks are evoked by naturalistic movie viewing.

1. Introduction

There is growing interest in studying brain function in response to naturalistic stimuli, for example, viewing film clips or listening to spoken narratives or music, as naturalistic experimental paradigms may evoke human cognition and behavior that more closely resembles "real-world" brain function (Hasson et al., 2004; Huth et al., 2016; Meer et al., 2020; Nishimoto et al., 2011; Sonkusare et al., 2019; Spiers and Maguire, 2007). Naturalistic stimulus paradigms during functional magnetic resonance imaging (fMRI) are emerging as a powerful tool to define brain imaging-based markers of psychiatric illness (Eickhoff et al., 2020), with several advantages in comparison to unconstrained resting state. Namely, studying brain network function during naturalistic stimuli may facilitate a deeper understanding of human brain function since the passive state is better constrained, and participant motion is reduced relative to unconstrained rest, which greatly increases the quality of the fMRI data. However, new analytical strategies are needed that assess both the shared rapid temporally evolving brain responses evoked by the naturalistic stimuli in participants, as well as idiosyncratic evoked signals in individual participants (Simony and Chang, 2020).

Both categorical and dimensional sources of variability can contribute to inter-subject variation in responses to naturalistic stimuli fMRI. In addition, while naturalistic stimuli paradigms provide better constraint of brain activity, there are challenges with modeling the evoked responses. Namely, evoked brain activity using conventional fMRI study designs and stimuli is relatively straightforward to model, whereas naturalistic stimuli are complex and dynamic, and it is much more difficult to generate a model of evoked activity for analyses. Data-driven methods that place no assumptions on the temporal course or

* Corresponding authors.
E-mail addresses: guoqiang.hu@mail.dlut.edu.cn (G. Hu), lisa_nickerson@hms.harvard.edu (L.D. Nickerson), cong@dlut.edu.cn (F. Cong).

https://doi.org/10.1016/j.neuroimage.2022.119193.
Received 31 May 2021; Received in revised form 23 February 2022; Accepted 6 April 2022
Available online 8 April 2022.

spatial pattern of brain activity obviate these challenges. Inter-subject correlation (ISC, Hasson et al., 2004) is one such data-driven approach for characterizing the consistency of brain responses across participants viewing the same naturalistic stimuli. For dynamic complex stimuli such as movies, ISC measures share information across brains by using each individual's measured brain activity to model another individual's brain activity. Using this strategy, the shared brain regions that respond to the same time-locked naturalistic stimuli across subjects can be estimated, even with stimuli that reflect complex dynamic real-life contexts (Hasson et al., 2004; Kauppi et al., 2014; Lerner et al., 2011; Nastase et al., 2019). Modifications to ISC include the temporal inter-subject functional correlation (ISFC), which considers the correlations between time courses from all possible pair-wise combinations of brain parcels across subjects (Simony et al., 2016), and the spatial ISC, which is an extension of temporal ISC to multi-voxel pattern analysis (Haxby et al., 2014; Norman et al., 2006).

Inter-subject representational similarity analysis (IS-RSA) is another technique that can be used to explore between-subject variability in the relationships between brain activity and behaviors (Finn et al., 2020; Kriegeskorte et al., 2008; Mantel, 1967; Meer et al., 2020). Van der Meer and colleagues (2020) explored the differences between movie viewing and resting state with Hidden Markov Models (HMM) and found that subject differences in brain state dynamics were linked to subjective movie ratings using IS-RSA. Through the study of between-subject variability, different schematic events (Baldassano et al., 2018) and different conditions when participants recall a movie (Chen et al., 2017, 2016) can be distinguished via the corresponding brain activity. In most cases, understanding patterns of brain states that are consistent across subjects as well as patterns that reflect inter-subject variability are of interest. In this study, we leverage a popular tensor decomposition method to simultaneously estimate spatial-temporal brain activity patterns that are shared across participants and that reflect inter-subject variability.

Generally, ISC-based methods are implemented with either a leave-one-out framework, in which one subject's time course is correlated with the average of all other subjects for each region, or a pairwise framework, in which correlation analysis is performed between each possible pair of subjects (Finn et al., 2020). A limitation of this computational procedure is that the resulting correlations are highly interdependent and violate the assumption of common parametric tests (Nastase et al., 2019), requiring careful attention to the inference method. In order to mitigate this limitation, we use a tensor component analysis (TCA) framework that characterizes spatio-temporal patterns that are shared across subjects as well as idiosyncratic features of evoked activity to naturalistic stimuli unique to different subjects, in a purely data-driven manner that assesses all brain networks simultaneously.

Tensor Component Analysis (TCA), also known as tensor Canonical Polyadic Decomposition (CPD,Kolda and Bader, 2009), is a fundamental model for tensor decomposition of multidimensional data with more than two dimensions. Assuming the data meet the assumption of a mixture model, in which signal sources undergo a linear mixing process, TCA more accurately estimates sources than matrix decomposition algorithms, and without any constraints (Williams et al., 2018). FMRI signals are innately multidimensional and can be naturally represented in tensor form. For example, a third-order fMRI tensor is organized as space × time × subjects (the order of modes does not impact the estimation). In TCA of the fMRI tensor, the spatial and temporal information regarding brain network activity evoked by different stimuli that is common to all participants exists in the first two dimensions. Subject loadings that capture between-subject variability exist in the third dimension.

TCA has demonstrated promise in a range of neuroimaging applications. It has been shown to have superior performance in identifying hidden signal sources when compared with 2-D matrix decomposition, e.g. principle component analysis (PCA) and independent component analysis (ICA), of multidimensional data (Williams et al., 2018). TCA has also been explored for magnetoencephalography (MEG) data analysis (Zhu et al., 2020a), and nonnegative constraint TCA applied to electroencephalography (EEG) time-frequency domain data was able to identify event-related (Cong et al., 2015a, 2015b; Wang et al., 2018) and naturalistic stimulus-evoked EEG responses (Zhu et al., 2020b). Mokhtari et al. (2019) investigated how different tensor organization and tensor decomposition methods applied to fMRI data impact the interpretation of dynamic functional connectivity. In our previous study (Hu et al., 2021), sparse constrained nonnegative TCA was proposed to estimate frequency specific coactivation patterns. TCA has also been applied to task fMRI data to explore additional dimensions of the data other than space and time, such as run and task condition (Andersen and Rayens, 2004), and has been adapted for multi-subject fMRI data analysis by placing spatial and temporal constraints to address inter-subject variability (Beckmann and Smith, 2005; Helwig and Hong, 2013; Kuang et al., 2020, 2015; Mørup et al., 2008; Zhou and Cichocki, 2012). We advance TCA for analysis of multi-subject fMRI data collected during naturalistic stimuli viewing by proposing a pipeline that does not place any constraints on the data and that enhances the reproducibility of the results.

We address three key issues that have limited the use of tensor decomposition for naturalistic stimuli fMRI (Wolf et al., 2010). First, the TCA algorithm may be slow or fail to converge, or have suboptimal convergence when applied to whole brain data. To mitigate this issue, the TCA is usually constrained in some way (Beckmann and Smith, 2005; Zhou et al., 2014). Instead of constraining the TCA algorithm, we propose instead to implement a parcellation strategy to reduce the data prior to TCA to facilitate convergence. Second, we propose a novel tensor spectral clustering method to enhance the reproducibility of the estimated components. Last, model order selection is always a challenge for tensor and matrix decomposition methods (Abou-Elseoud et al., 2010; Beckmann, 2012; Kuang et al., 2018). Here we propose to select the model order based on component reproducibility assessed via our novel spectral clustering method. The effectiveness of the proposed framework is first demonstrated with simulated and traditional task fMRI, in which we know the ground truth stimulation time courses (and hence have a model of the brain activity). We then apply the proposed framework to fMRI data collected during movie watching, in which there is no *a priori* model of brain activity, to identify spatial brain networks engaged during the task. Analysis of both task fMRI and naturalistic stimuli fMRI results show that the proposed method has several advantages compared with the widely used ISC method.

The rest of the paper is structured as follows. In section 2, Materials and Methods, we present the TCA model that was used to estimate spatio-temporal shared components, e.g., the decomposition algorithm used in this paper, the criteria that were used to evaluate the reproducibility of estimated components and the model order selection method, and the test datasets. In section 3, Results, we show results using simulated data and motor task fMRI. After establishing the robustness of the proposed framework from simulations and conventional task fMRI, we show results from application of our analytic approach to two different naturalistic stimuli fMRI datasets: one in which participants watched a short 82 second montage of scenes, collected from 184 participants by the Human Connectome Project (HCP), and one in which participants watched a longer movie (20 minutes), collected from 17 participants by Meer et al. (2020). In sections 4 and 5, the Discussion and Conclusions, respectively, we discuss the benefits and pitfalls of our proposed approach and the conclusions from our work. The mathematical foundation of tensor spectral clustering used to evaluate the stability of estimated components is provided in the Appendix.

2. Materials and methods

2.1. TCA model

Our proposed application of TCA of naturalistic stimuli fMRI data proceeds in three steps as shown in Fig. 1. First, a data reduction step is introduced in which the activity of node (or region) time courses is ex-

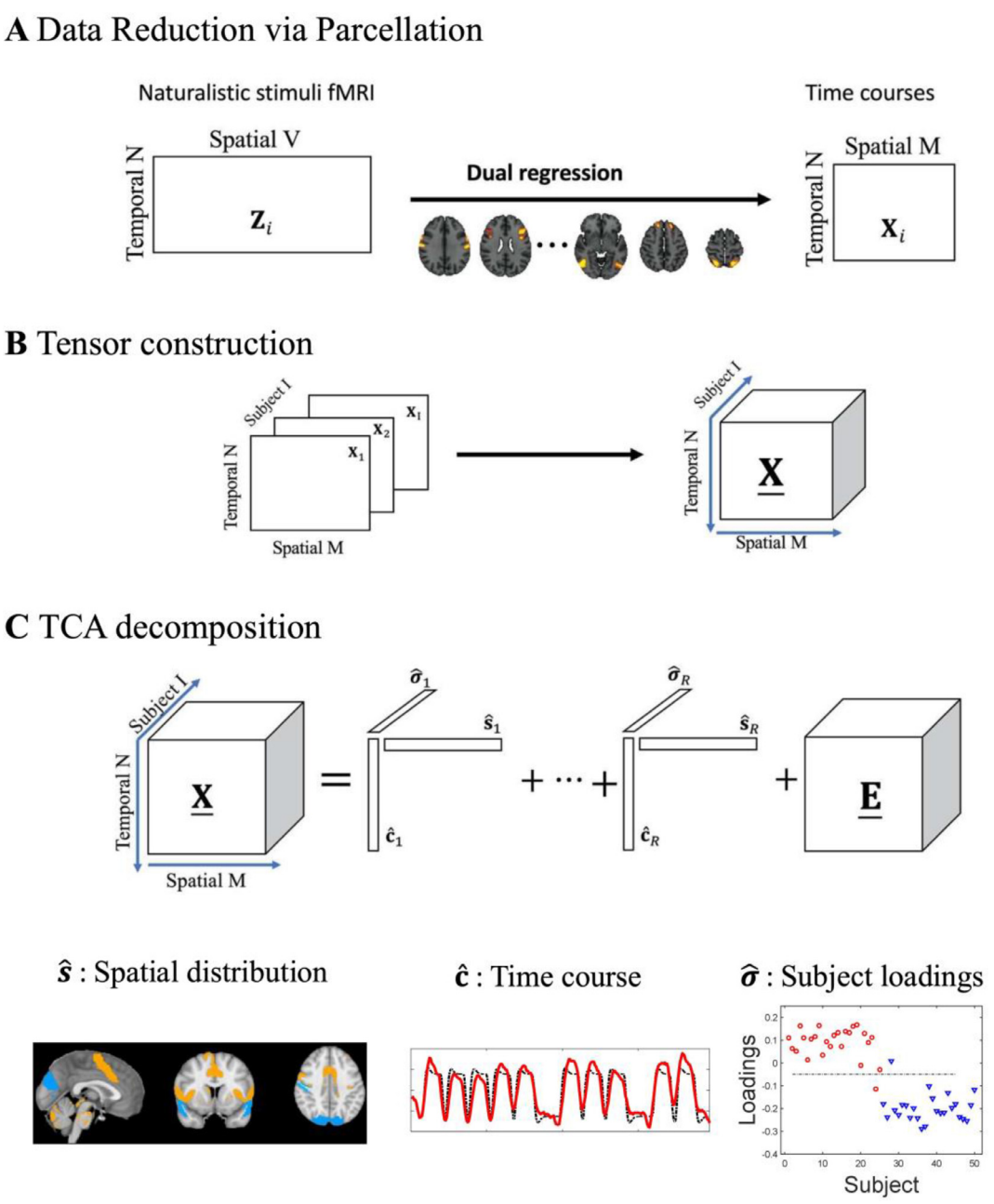

Fig. 1. Tensor component analysis pipeline. (A) Estimating node timeseries with dual regression from standard preprocessed dense data. (B) Stacking all subjects' node data to construct a tensor. (C) Extracting tensor components with tensor component analysis. The estimated components of each mode $\hat{s}$, $\hat{c}$, $\hat{\sigma}$ correspond to the spatial distribution, time course and subject loadings, respectively.

tracted from the naturalistic stimuli fMRI data using an open-access parcellation scheme derived from independent component analysis (ICA) of resting state fMRI; next, the time courses from all participants are stacked to construct a third-order fMRI tensor; last, TCA is applied to estimate spatio-temporal patterns and their corresponding subject loadings.

In the first step, rather than applying TCA to voxel-wise fMRI data, a whole brain parcellation scheme is applied to extract node time courses for the TCA. This is done for several reasons. First, BOLD signals are expected to be correlated across neighboring voxels and, with an appropriate parcellation method, node time courses will have a higher signal noise ratio (SNR) compared with the SNR of time courses from dense data (Glasser et al., 2016). Parcellation schemes based on ICA of fMRI data with high model orders (>100 to several hundred) will be comprised of components that feature individual small brain regions, bilateral brain regions, or sparse sub-networks that may have regions overlapping other components (e.g., reflecting hubs such as posterior cingulate cortex), and can thus be considered as nodes for use in network analysis (Smith, 2012). Several studies have demonstrated that brain parcellation with spatial ICA demonstrates better performance for network modeling compared with other parcellation methods (Smith et al., 2011; Arslan et al., 2018), with higher model orders providing better performance (Pervaiz et al., 2020). In this study, a brain parcellation scheme derived from ICA of the Human Connectome Project (HCP, Van Essen et al., (2013)) resting state fMRI data with model order of 300 (provided by the HCP, Smith et al., 2011) is used to extract node time courses for TCA. The time courses are extracted via the first stage of dual regression (Nickerson et al., 2017) in which the

full set of ICA components, $\mathbf{S}_{\mathrm{ICA}}$, are regressed against each participant's 4D fMRI data (e.g., multivariate spatial regression) to extract the time courses. This is different from how conventional binary parcellation masks are used to extract average time courses from each node in that the multivariate spatial regression accurately handles any potential spatial overlap among the ICA maps due to individual brain regions participating in more than one brain network (or sub-network) represented in the ICA maps. The analysis code for the tensor component analysis framework is available at https://github.com/GHu-DUT/Tensor-components-analysis-for-naturalistic-stimuli-fMRI.

2.1.1. Multilinear mixing model

For naturalistic fMRI we assume, similar to the ISC model (Finn et al., 2020; Nastase et al., 2019), that time courses $\mathbf{C} \in \mathbb{R}^{N \times J}$ and spatial patterns $\mathbf{S} \in \mathbb{R}^{M \times J}$ of nodes in the parcellation are stimulus-evoked responses that are consistent across subject. N is the number of timepoints, J is the number of patterns, M is the number of nodes. Thus, in our TCA-based model, for each pattern j, the loading $\boldsymbol{\sigma}_{i,j}$ for subject i is different from other subjects. In this case, for subject i, the node time courses, $\mathbf{X}_i \in \mathbb{R}^{M \times N}$, can be represented as:

$$\mathbf{X}_i = \mathbf{S} \times \mathbf{diag}\left(\boldsymbol{\sigma}_{i,:}\right) \times \mathbf{C}^T + \mathbf{Id}_i + \boldsymbol{\epsilon}_i, \tag{1}$$

where $\mathbf{Id}_i$ are stimulus-evoked responses that are idiosyncratic to each subject and $\boldsymbol{\epsilon}_i$ corresponds to noise, which may reflect spontaneous neural activity and non-neural physiological and scanner signal sources. $\mathbf{diag}(\boldsymbol{\sigma}_{i,:})$ is a square matrix of order J with $\boldsymbol{\sigma}_{i,:}$ on the diagonal and other elements of the matrix equal to zero.

2.1.2. Tensor construction

A tensor is constructed by stacking the multi-subject data, $\mathbf{X}_i$, to create $\underline{\mathbf{X}} \in \mathbb{R}^{M \times I \times N}$, with I equal to the total number of subjects. Although the spatial and temporal patterns are assumed to be shared across participants, the loadings on the components in each participant are different. Of note, the model also does not place any assumptions on the distribution of time courses or spatial distributions.

2.1.3. TCA unmixing model

TCA is a basic model for tensor decomposition that is unconstrained. With different constraints, different algorithms can be derived, including non-negative canonical polyadic decomposition (NCPD) (Zhou et al., 2014) and independent constrained CPD (e.g. tensor-ICA Beckmann and Smith, 2005). In the TCA model, a third-order tensor $\underline{\mathbf{X}}$ can be represented as the sum of several rank-1 tensors and a residual tensor $\underline{\mathbf{E}}$ (Hitchcock, 1927), which is illustrated in Fig.1 (C). The mathematical formula is as follow:

$$\underline{\mathbf{X}} = \sum_{r=1}^{R} \hat{\mathbf{s}}_r \circ \hat{\boldsymbol{\sigma}}_r \circ \hat{\mathbf{c}}_r + \underline{\mathbf{E}} = \sum_{r=1}^{R} \underline{\mathbf{X}}_r + \underline{\mathbf{E}}, \tag{2}$$

where vectors $\hat{\mathbf{s}}_r \in \mathbb{R}^{M \times 1}$, $\hat{\boldsymbol{\sigma}}_r \in \mathbb{R}^{I \times 1}$ and $\hat{\mathbf{c}}_r \in \mathbb{R}^{N \times 1}$ are r^{th} estimated tensor component (TC) spatial distribution $\mathbf{S}$, subject loadings $\boldsymbol{\sigma}$ and time courses $\mathbf{C}$ respectively. The operator $\circ$ represents the outer product of vectors. $\underline{\mathbf{X}}_r$ represents the rank-1 tensor that constructed by the corresponding components of each mode. The idiosyncratic stimulus-evoked responses, spontaneous signals and noise signals are contained in the residual tensor $\underline{\mathbf{E}}$ and R is the number of extracted patterns. Ideally, the number of tensor components, or model order, should be equivalent to the number of patterns, J, shared across subjects. However, in real-world applications, the number of spatio-temporal patterns is unknown. In the present study, we propose a novel method for determining model order according to stability of tensor spectral clustering. Once a solution is identified, for each tensor component, the spatial distributions are $\hat{\mathbf{s}}_r$, time courses are $\hat{\mathbf{c}}_r$. These are the same across subjects, with subject loadings, $\hat{\boldsymbol{\sigma}}_r$, reflecting between-subject variation in the strength of the patterns.

2.2. TCA estimation algorithm

The alternating least-squares (ALS) algorithm (Cichocki et al., 2015; Kolda and Bader, 2009) is used to estimate factor matrices $\mathbf{S}$, $\mathbf{C}$ and $\boldsymbol{\sigma}$. The ALS algorithm proceeds by fixing two of the factor matrices to optimize over the third factor matrix. For example, while time courses, $\mathbf{C}$, are being estimated, the spatial patterns, $\mathbf{S}$, and subject loadings, $\boldsymbol{\sigma}$, are fixed. The time courses are updated with the following rule:

$$\mathbf{C} \leftarrow \mathrm{argmin}_{\tilde{\mathbf{C}}} \frac{1}{2} \left| \underline{\mathbf{X}} - \sum_{r=1}^{R} \hat{\mathbf{s}}_r \circ \hat{\boldsymbol{\sigma}}_r \circ \hat{\mathbf{c}}_r \right|_F^2, \tag{3}$$

where F represents the Frobenius norm. The updating rule is solved as a linear least-squares problem that is convex and has a closed-form solution. The other factor matrices are solved with the same updating rule and the three factor matrices are updated in an alternating fashion until the stop criteria is met, in this case when the absolute difference of the fits between two adjacent iterations is less than 1e-8, or when the number of iterations exceeds 1000. The ALS algorithm is provided open access from the tensor toolbox (https://www.tensortoolbox.org).

2.3. Model order selection via tensor spectral clustering

Similar to ICA, model order (number of extracted components) selection is a significant methodological concern when applying these data driven algorithms for fMRI data analysis (Abou-Elseoud et al., 2010; Beckmann, 2012; Kuang et al., 2018). Information-theoretic criteria (ITC) have been used in numerous signal processing applications to estimate model order, including minimum code length based minimum description length (MDL) criterion (Rissanen, 1978), Akaike information criterion (AIC) (Akaike, 1998), and Bayesian information criterion (BIC) (Rissanen, 1978). However, studies have demonstrated that estimations based on different criteria may be different and these criteria may lose efficacy when the signal noise ratio is low (Cong et al., 2011; Hu et al., 2020). In this study, model order is selected based on reproducibility of the decomposition results. We use the reproducibility of the estimated rank-1 tensor $\underline{\mathbf{X}}_r = \hat{\mathbf{s}}_r \circ \hat{\mathbf{c}}_r \circ \hat{\boldsymbol{\sigma}}_r$ via a novel tensor spectral clustering approach to select the model order. In this case, the tensor decomposition is done for a range of model orders, the algorithm stability under each model order is evaluated via tensor spectral clustering, and the model order with the highest algorithm stability index is selected as the appropriate decomposition.

In the stability analysis, for the given dataset, the same algorithm with the same parameters is ran K times, each with different initial conditions. For each model order, R, $R \times K$ components are estimated across runs for each mode (temporal, spatial, subject). The similarity matrices (or adjacency matrices calculated by correlating each pair of components for a mode) for each mode $\mathbf{W}^{(\mathbf{S})}$, $\mathbf{W}^{(\boldsymbol{\sigma})}$, $\mathbf{W}^{(\mathbf{C})} \in \mathbb{R}^{RK \times RK}$ are then fed into tensor spectral clustering, which is a co-clustering method that enables fusing and assessing the stability information of different modes simultaneously. Details of the formulation for tensor spectral clustering are provided in the Appendix. In tensor spectral clustering, the number of clusters is set to equal number of extracted components R. Stable components will form a tight cluster, with a stability index quantified as the average of the intra-cluster similarities. Ideally, if the estimated components for a given model order are stable, the intra-cluster similarity of the corresponding cluster is close to 1, whereas the stability index for unstable components will be close to 0. The algorithm stability is defined as the average of component stability indices.

2.4. Simulations

We demonstrate the effectiveness of the proposed framework using numerical simulations performed in MATLAB. The simulated spatial maps and time courses for 29 ICA components (SimBT (Erhardt et al., 2012) http://mialab.mrn.org/software) and time courses

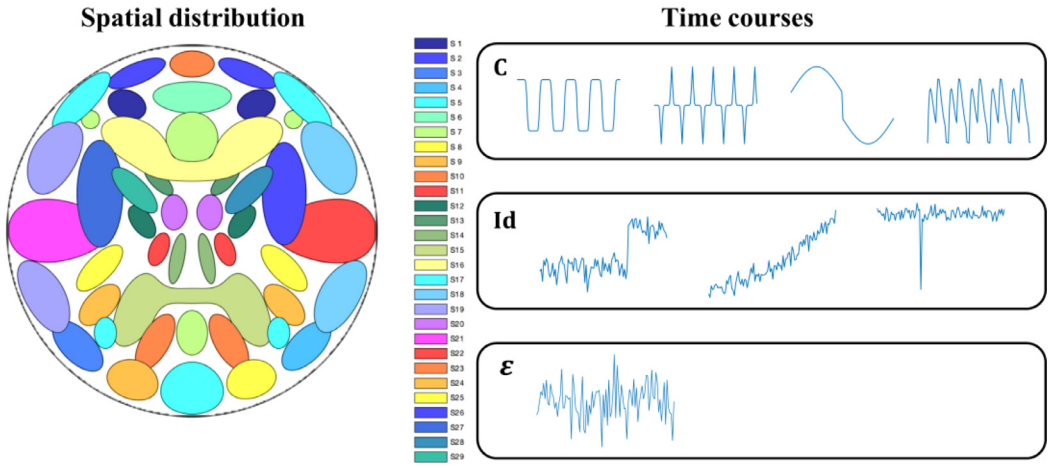

Fig. 2. Ground truth spatio-temporal signal sources used in simulations. The left figure shows the spatial distribution of 29 ICA components. The right column shows time courses for consistent components across subjects (the first row, $\boldsymbol{C}$), idiosyncratic components (the second row, $\boldsymbol{Id}$) and for spontaneous components (the third row, $\boldsymbol{\epsilon}$).

(http://mlsp.umbc.edu/simulated_fmri_data.html) are shown in Fig. 2. Four components were simulated to represent consistent spatio-temporal signals across subjects (with time courses shown in the first row of Fig. 2). There are also three idiosyncratic components for each subject, similar to scanner or motion artifacts present in fMRI data (second row of Fig. 2). These components were given a random circular shift for each subject. Time courses in the third row of Fig. 2 represent spontaneous brain activity included in the simulations. Different spontaneous components were generated independently for each subject following a Gaussian distribution. The total signal noise ratio (SNR) was fixed at 2dB. We generated a random node weight matrix $\mathbf{S} \in \mathbb{R}^{29 \times 8}$ and subject loading matrix $\boldsymbol{\sigma} \in \mathbb{R}^{10 \times 8}$ to generate 10 participant datasets using equation (1). All subject's data were then stacked to construct a three-order tensor $\underline{\mathbf{X}}_{\text{Simulation}} \in \mathbb{R}^{29 \times 10 \times 100}$. This tensor was then decomposed with model orders ranging from 2 to 10. Under each model order, the TCA algorithm was run 20 times and the stability index was calculated with tensor spectral clustering. The correlation coefficients between the estimate components for the model order with the highest stability index and the corresponding ground truth were used as a criterion to evaluate the performance of the proposed framework.

2.5. Motor task fMRI experiment

The effectiveness of the proposed framework is also demonstrated with conventional motor task fMRI in which we know the ground truth stimulation time courses that can be used to model the brain task activity. Motor task fMRI data from 100 healthy unrelated subjects (22-36 years) were utilized from the WU-Minn Human Connectome Project (HCP; Van Essen et al., 2013). During the motor task, participants were presented with visual cues to either tap their left or right fingers, squeeze their left or right toes, or move their tongue. Blocks for each movement type lasted 12 seconds and were preceded by a 3 second cue. For each subject, a total of 284 timepoints were collected with TR=0.72s. Additional details of the motor task for the HCP are provided in Barch et al. (2013).

2.5.1. Preprocessing

The fMRI data went through the HCP's standard minimal preprocessing pipeline (motion correction, distortion correction, high-pass filtering (200s), and nonlinear alignment to MNI template space (Glasser et al., 2013)).

2.5.2. GLM

In order to evaluate the performance of TCA, we used the standard GLM as the gold standard, which was applied to the same data. A conventional mixed-effects GLM analysis was conducted to derive activation estimates for each reference function, as described in Barch et al. (2013). Five predictors were included in the Motor model — right hand, left hand, right foot, left foot, and tongue. Time courses of visual cues for each type of movement were convolved with Hemodynamic Response Function (HRF) and low-pass filtered with a high-frequency cutoff of 0.5 Hz. Spatial maps of linear contrasts (Cues, Foot, Tongue, Hand) of the parameter estimates were computed to compare each condition to baseline. Higher level GLMs, including age and sex as covariates, were used to estimate the spatial distributions of tongue, foot and hand movement and total movement evoked brain activity via one sample t-tests of the contrast of parameter estimate maps, with a correction for multiple tests to control the family-wise error (FWE). Since the evoked response to the motor mapping task was so strong (Barch et al., 2013), a higher threshold ($p<0.001$) was used.

2.5.3. TCA

Following the recommendations of Pervais et al. (2020), a higher model order functional parcellation based on spatial ICA components was used as the parcellation scheme for our study. Spatial ICA components provided by the HCP with a model order of 300 were used as templates with dual regression (Nickerson et al., 2017) to derive the subject-specific time courses of each node, as shown in Fig. 1 (A). Post-processing of time courses included: (1) removal of the first 10 time-points (2) demeaning, (3) detrending linear, quadratic and cubic trends, and (4) variance normalization. The time courses for each node for each subject were then stacked in the subject dimension to create a tensor, $\underline{\mathbf{X}}_{\text{Motor}} \in \mathbb{R}^{300 \times 100 \times 284}$. The tensor was then decomposed with TCA, with model orders ranging from 2 to 20. The decomposition was repeated 20 times for each model order to calculate the reproducibility of the estimated components and the model order via our proposed tensor spectral clustering strategy. Task-related TCA components were identified via similarity of component time courses to the "ground truth" time courses from the GLM analyses.

2.5.4. ISFC

We compared our approach with another popular approach for naturalistic fMRI data analysis, ISFC (Simony et al., 2016). ISFC was calculated with a sliding window of 20s (28 TRs). At each time point,t, the pairwise correlations between all nodes were calculated over the window interval (t, t+20) to construct a correlation matrix for time point t. Correlation matrices were computer for each window shifted by 0.72s (1 TR) in time. The resulting sliding window correlation matrices were then analyzed with k-means clustering, with the number of clusters set

from 2 to 20. For each k-means run, cluster indices of each timepoint were used to represent the occurrence of each task-related brain state (cluster). The spatial distributions of each brain state were derived by calculating the average connectivity of each node with all other nodes in the cluster. The time course of each state is calculated as the average occurrence across subjects. For ISFC, "ground truth" time courses were assumed to be the GLM stimulation time courses convolved with the HRF and the sliding window.

2.6. Naturalistic stimuli fMRI experiment

We used a naturalistic fMRI dataset that was also collected by the HCP (Van Essen et al., 2013). Healthy adult participants (aged 22-35 years) underwent fMRI using a 7 T Siemens Magnetom scanner (voxel size = 1.6mm^3, TR = 1s) during a movie-watching paradigm. The sample used here (n = 184) reflects all available data for this paradigm. Each subject underwent four runs of 15-min movie watching (MOVIE1-MOVIE4). Each run comprised five video clips presented in a fixed order. FMRI data were also collected during a validation clip (the fifth video clip), consisting of a brief montage (1min 22s) of moving scenes depicting people and landscapes. The music played along with the movie scenes contained features to evoke consistent brain activity across participants (Alluri et al., 2012). Five music features (Fluctuation Centroid, Fluctuation Entropy, Key Clarity, Mode and Pulse Clarity) were extracted using the MIRToolbox (Lartillot, O., 2007). These music features facilitate the interpretation of the estimated tensor components. In addition, this movie included a social scene. To demonstrate relationships between inter-subject variability in TCA components with behavior and facilitate interpretation of results, the subject loadings on social scene-related TCA components were assessed for correlations with behavioral measures from the Semi-Structured Assessment for the Genetics of Alcoholism (SSAGA; BUCHOLZ et al., 1994; Hesselbrock et al., 1999) and NIH Toolbox. We selected seven measures related to social function, including Friendship, Loneliness, Perceived Hostility, Perceived Rejection, Emotional Support, Instrumental Support and Antisocial Personality Problems Raw Score.

All fMRI analyses utilized the FIX-denoised data that underwent standard HCP minimal preprocessing (motion correction, distortion correction, high pass filtering, and nonlinear alignment to MNI template space (Glasser et al., 2013)) plus regression of 24 framewise motion estimates (six rigid-body motion parameters and their derivatives and the squares of those 12) and regression of confound components identified via ICA (Griffanti et al., 2014; Salimi-Khorshidi et al., 2014). Details of data acquisition and basic data preprocessing can be found in previous studies (Glasser et al., 2013; T. Vu et al., 2016; Van Essen et al., 2012).

Both TCA and ISC were applied to same FIX-denoised dataset. TCA was implemented exactly the same way as for the analysis of the motor task fMRI data (shown in Fig. 1), with the resulting tensor, $\underline{\mathbf{X}}_{\text{Naturalistic}} \in \mathbb{R}^{300 \times 184 \times 82}$, decomposed with our TCA approach. ISC was also applied to the HCP naturalistic stimuli fMRI to compare the performance of TCA and ISC. In ISC, the same parcellation strategy used for the TCA framework was also applied. In ISC framework, IS-RSA was used to evaluate the relationship between shared brain networks across subjects and subject traits. For each subject pair, brain similarity was calculated as the correlation of activity time courses. Behavioral similarity was calculated according to absolute value of the difference in behavioral data of subject pair. Representational similarity was assessed by calculating correlation between the brain and behavioral similarity matrices. Details of IS-RSA can be found in the previous study (Finn et al., 2020; Kriegeskorte et al., 2008; Mantel, 1967; Meer et al., 2020).

In order to demonstrate that our proposed framework is also suitable for naturalistic stimuli with longer durations, we used the naturalistic stimuli fMRI data provided by Meer et al. (2020), which implemented a paradigm with 20 min movie stimuli (The Butterfly Circus). FMRI data were collected with identical movie stimuli on two separate occasions (Movie view A and Movie view B) with an interval of three months between sessions. 17 participants completed both movie viewing sessions. Two participants were excluded because of in-scanner head motion. The fMRI data was collected with TR of 2200msec and 535 volumes were acquired. Standard preprocessing was performed using fMRIPrep (Esteban et al., 2019) and included slice-timing, motion correction, co-registration to the structural image, spatial normalization to MNI space, and spatial smooth with a 6 mm Gaussian kernel. ICA-AROMA was subsequently performed using non-aggressive denoising. Details of the data collection, pre-processing, and brain state dynamics can be found in Meer et al. (2020). The Butterfly Circus narrates an intense, emotionally evocative story of a man born without limbs who is encouraged by the showman of a renowned circus to overcome obstacles of self-worth and reach his own potential. Annotations for (i) the use of language, (ii) change of scenes, (iii–v) Positive/Negative Faces, and (vi–viii) Positive/Negative Scenes during the movie are also provided. Meer et al. (2020) applied a hidden Markov model (HMM) to identify brain states dynamics for 14 canonical brain networks (BN) derived with group ICA (Shirer et al., 2012). In order to compare the results with the findings of Meer et al. (2020), we used the same set of BNs for parcellating the fMRI data. The first 5 time points for each BN average temporal course were discarded. Thus, for each subject we obtained a matrix (530×14) for each movie viewing session. The matrices for movie viewing A and movie viewing B were then stacked and concatenated in the subject dimension to construct the tensor, $\underline{\mathbf{X}} \in \mathbb{R}^{30 \times 530 \times 14}$, that was decomposed via our TCA approach.

3. Results

3.1. Simulations

Fig. 3 shows the simulation results. Fig. 3(A) shows the algorithm stability indices for the different model orders. We found that the algorithm stability curve reached its peak at model orders of 3 and 4. To extract more information about the simulated brain responses, results at model order 4 were further analyzed. Note that the algorithm stability index at this model order is 1, which means all components estimated at that model order are the same for all 20 runs, indicating that all the components are reproducible. The spatial distributions, time courses and subject loadings for each component are shown in Fig. 3(B-E). Based on the correlation coefficient between estimated component time courses and spatial maps with the ground truth time courses and spatial maps, all four components are successfully estimated. In order to highlight the activated and deactivated brain regions, the spatial distribution of the estimated component is shown with a proportional threshold of 5% (Garrison et al., 2015), with warm colors representing activation (relative to the within-component global average) and cool colors representing deactivation (relative to the within-component global average) within each component.

3.2. Motor task fMRI experiment

For motor task fMRI data, for TCA, the algorithm stability curve reached a peak at model order of 4. Hence, the estimated TCA components with model order of 4 were selected for further analysis. For ISFC, the number of clusters is selected as 6. With this number of clusters, the estimated time courses have the greatest similarity to the corresponding ground truth time courses.

The spatial distributions and time courses of the estimated components, and the results from applying the GLM and ISFC for analysis are shown in Fig. 4, with display and thresholding at $|Z| > 2.3$ after transformation into Z-scores across the spatial domain, and warm colors representing activation and cool colors representing deactivation. For each component, after normalization, both stimulus timing and estimated time courses are demonstrated in the same subfigure to identify of the estimated components. In the experiment, the embedded components that correspond to the tongue, foot and cues are successfully

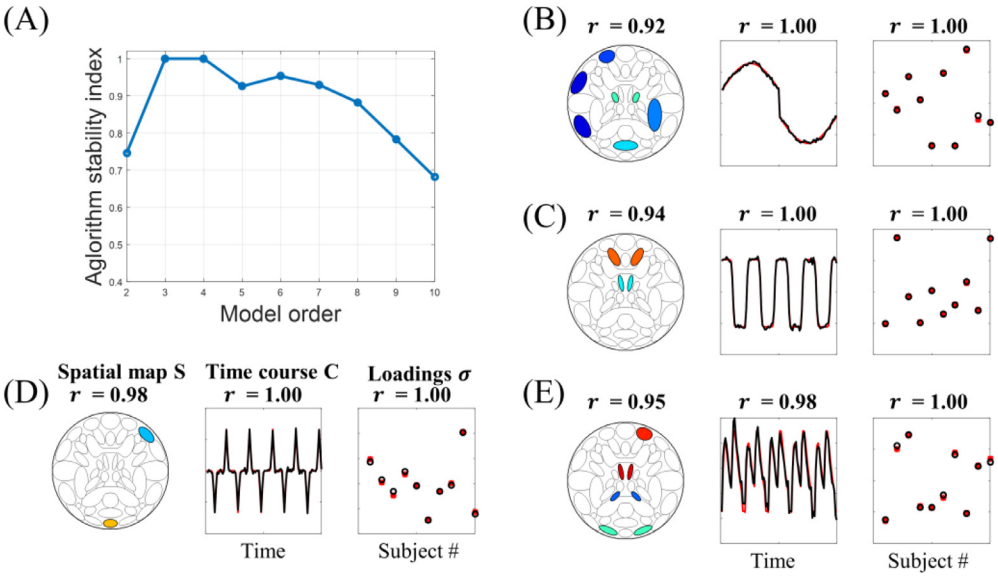

Fig. 3. Simulation results. (A) Algorithm stability index for different model orders. The algorithm reaches the greatest stability at model order of 4, which is exactly the same as the number of consistent components. (B) - (E) estimated components and ground truths signals. r is the correlation coefficient between the estimate component spatial map/time course and the corresponding ground truths. For spatial distributions, a proportional threshold of 5% (Garrison et al., 2015) was used, with warm colors representing activation (relative to the within-component global average) and cool colors representing deactivation (relative to within-component global average) within each component. For time courses, the red represents ground truth and the black indicates estimations.

estimated. However, the component corresponding to hand movements failed to be detected by TCA, which is due to poor temporal consistency across subjects (see Supplementary Fig.1). E.g., components with worse consistency across subjects will reduce algorithm stability and, in turn, the model order that may reveal such components will not be selected as the final model order.

Inspection of the spatial maps and time courses in Fig. 4 shows that the estimation of spatial distributions of activation are very consistent across methods. Comparison of the estimated time courses of the visual cues from TCA and ISFC shows that the TCA time courses resemble the visual cues after being convolved with hemodynamic response function. The time courses of ISFC are similar to the stimulation time course convolved with the sliding window, which results in a distorted representation for the visual cues (Fig. 4 (A)). Such distortions may hinder the investigation of the relationship between brain activity and movie features in naturalistic stimuli. However, ISFC successfully estimated the spatial map and time course of the hand movements whereas TCA did not at this model order (see Supplementary Fig. 2).

3.3. Naturalistic stimuli fMRI experiment

For the short naturalistic stimuli fMRI from the HCP, the TCA algorithm reaches the highest stability at model order equal to 3 and all three tensor components estimated under this model order are highly reproduced (see Supplementary Fig. 3). The estimated components under this model order were selected for further analysis.

The spatial distribution of the first tensor component estimated with TCA and the corresponding map estimated by ISC analyses of these data are shown in Fig. 5 (A). Bilateral occipital fusiform gyrus, lingual gyrus and superior temporal gyrus are identified as activated regions in both the TCA component and the ISC spatial map. However, bilateral postcentral gyrus, superior parietal lobule and left precentral gyrus are also identified as activated in the ISC map, but not in the TCA component. Bilateral cerebellum and lateral occipital cortex are activated in the TCA component.

Fig. 5 (B) shows a bar plot of the average correlation coefficients between the subject time courses extracted from the lingual gyrus and temporal gyrus, and the temporal course of the TCA component. This shows that the time course of lingual gyrus is negatively correlated with the estimated TCA component time course, whereas the time course of the temporal gyrus is positively correlated with the estimated time course. This opposite response to the movie stimuli of the lingual gyrus and temporal gyrus is not identified by ISC. Fig. 5 (C) shows the estimated time course of the first tensor component with the onset of the annotated stimuli in the movie to illustrate the relationship between them. Inspection of the timing suggests that landscape scenes result in increases in BOLD signal for this mode, while scenes with social content are associated with decreases in BOLD signal. In an exploratory analysis, we applied the proposed framework on a social cognition task fMRI from the HCP dataset. Then we compared the spatial distribution between social task evoked brain network (Supplementary, Fig. 8) and the movie stimuli evoked component, and found that the social task network was significantly correlated ($r = 0.27$, $P = 10^{-6}$) with the TCA component. The network estimated with ISC was also significantly correlated with the social task evoked brain network ($r = 0.28$, $P = 10^{-6}$). Correlations between the subject loadings for the TCA component and the behavioral measures related to social function showed a significant correlation (FDR corrected, $P<0.05$) between TCA component loadings and antisocial personality score (Fig. 5 (D)). A significant correlation ($r = 0.02$, $P = 0.01$) between antisocial personality scores and shared brain activities across subjects estimated with ISC is also identified with IS-RSA but the correlation coefficient is only 0.02.

The time course of the second tensor component was significantly correlated with the music feature Pulse Clarity ($r = 0.39$, $P = 10^{-4}$), as shown in Fig. 5(E). But the time courses estimated with ISC failed to correlated with the music feature ($r = 0.19$, $P = 0.10$). All three estimated tensor component spatial maps show effects in bilateral cerebellum, occipital fusiform gyrus, and lateral occipital cortex. The lingual gyrus is deactivated in the first TCA component, but not in the second or third components. Left frontal pole, which does not appear in the first TCA component, is deactivated in both the second and third TCA components, and the bilateral superior temporal gyrus is activated in the first and second TCA components, but not the third. Thus, TCA is able to identify overlapping brain activation modes.

Fig. 6 demonstrates that our proposed framework is also suitable for fMRI data with long-duration movie stimuli. Three components were estimated with TCA. The spatial distributions show a strong correlation with the spatial distributions reported in Meer et al. (2020) using HMM (correlation indicated above each map). The first TCA component corresponds to the language state estimated with the HMM ($r = 0.86$, $P = 10^{-5}$). The time course of the component was significantly correlated with annotation of the use of language (convolved with HRF, $r = 0.12$, $P = 0.006$), as shown in Fig. 6 (A). The second component corresponds to an interoception state ($r = 0.72$, $P = 0.004$) and the third component corresponds to task-positive network ($r = 0.88$, $P = 10^{-5}$).

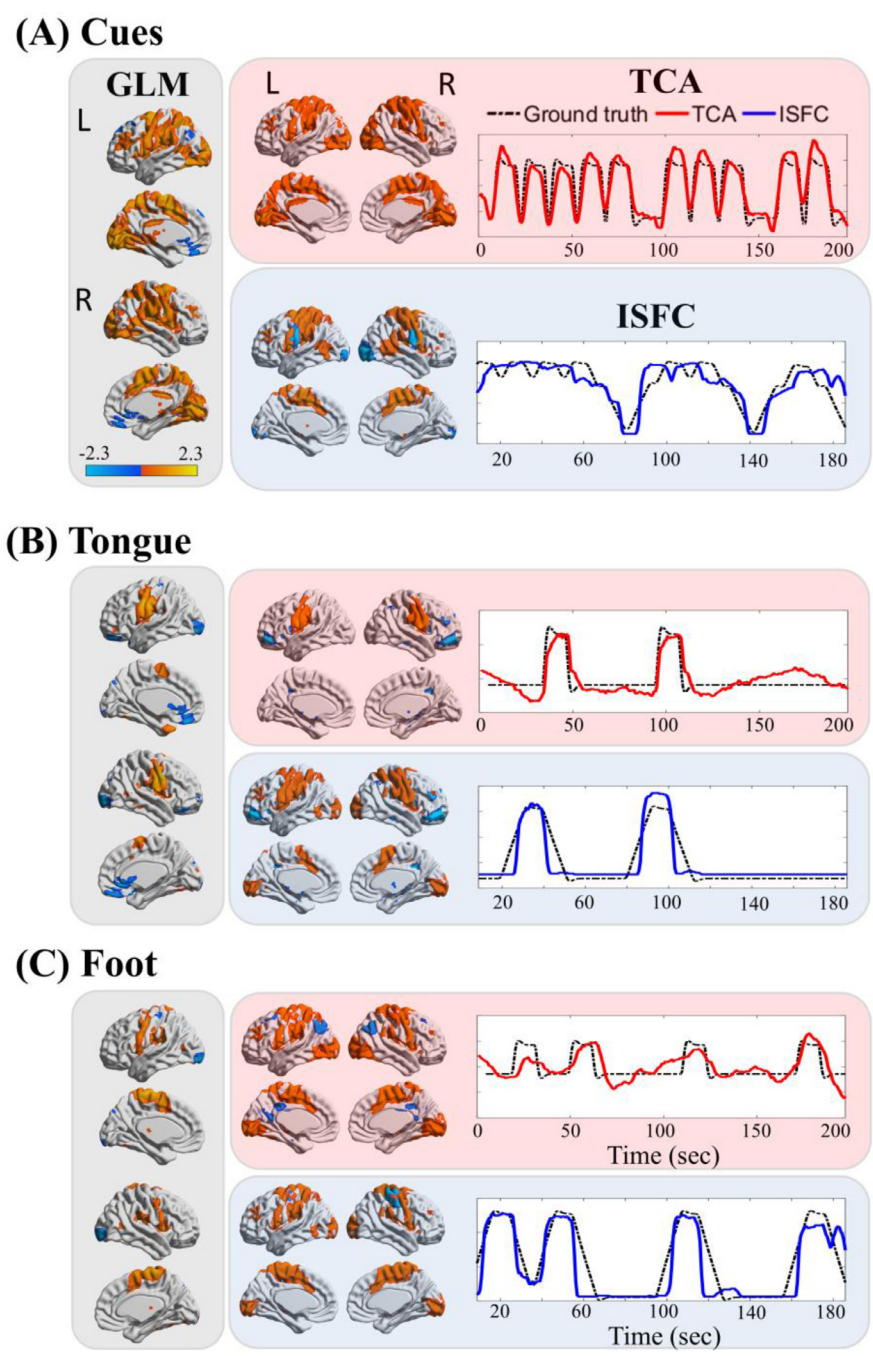

Fig. 4. Comparison of TCA, GLM and ISFC. For spatial distributions, warm colors represent activation (relative to within-state global average) while cool colors represent deactivation (relative to within-state global average) within each state. In the plots of the time courses, the red lines represent estimated time courses with TCA, blue lines are the estimated time courses with ISFC, and the black dash lines represent the ground truth time courses. Note that for TCA, the ground truth time courses are the experiment stimulus time course convolved with the HRF, which is the theoretical neural response of the task. For ISFC, the ground truth time courses are the experiment stimuli time courses convolved with the sliding window (28TRs).

The occupancy of these three components was shown to be higher during movie watching than during resting-state (Meer et al., 2020), which demonstrates that TCA can estimate brain activity evoked with naturalistic stimuli distinct from spontaneous brain activity. We also found that subject loadings during movie viewing B are lower than for movie viewing A, so even though similar spatial and temporal patterns of activity are evoked with repeated stimuli, differences in brain activation corresponding to repeated viewing of the same stimuli can also be assessed with TCA. Last, we evaluated the relationship between subject loadings and scores from the post-movie questionnaires that were administered to participants and found that subject loadings on the first tensor component for movie viewing B were significantly correlated with boredom ($P = 0.02$, uncorrected), which may explain the smaller subject loadings reflecting reduced strength on this pattern during the repeat viewing.

4. Discussion

In this study, an analysis framework for applying TCA to fMRI data to discover spatio-temporal components that are shared across subjects during naturalistic movie viewing was proposed. In this framework, a third-order tensor is constructed from the timeseries extracted from all brain regions from a given parcellation, for all participants. This tensor is then decomposed via TCA to identify modes corresponding to the spatial distribution (maps) and time series that are common to all participants, and subject loadings that reflect between-subject variability in the patterns of brain activation in response to naturalistic stimuli. The stability of the extracted components is evaluated with a novel clustering method, tensor spectral clustering, to guarantee the reproducibility of the results. Model order is selected based on the stability of the results across a range of model orders. Extensive testing (Figs. 3–5 and

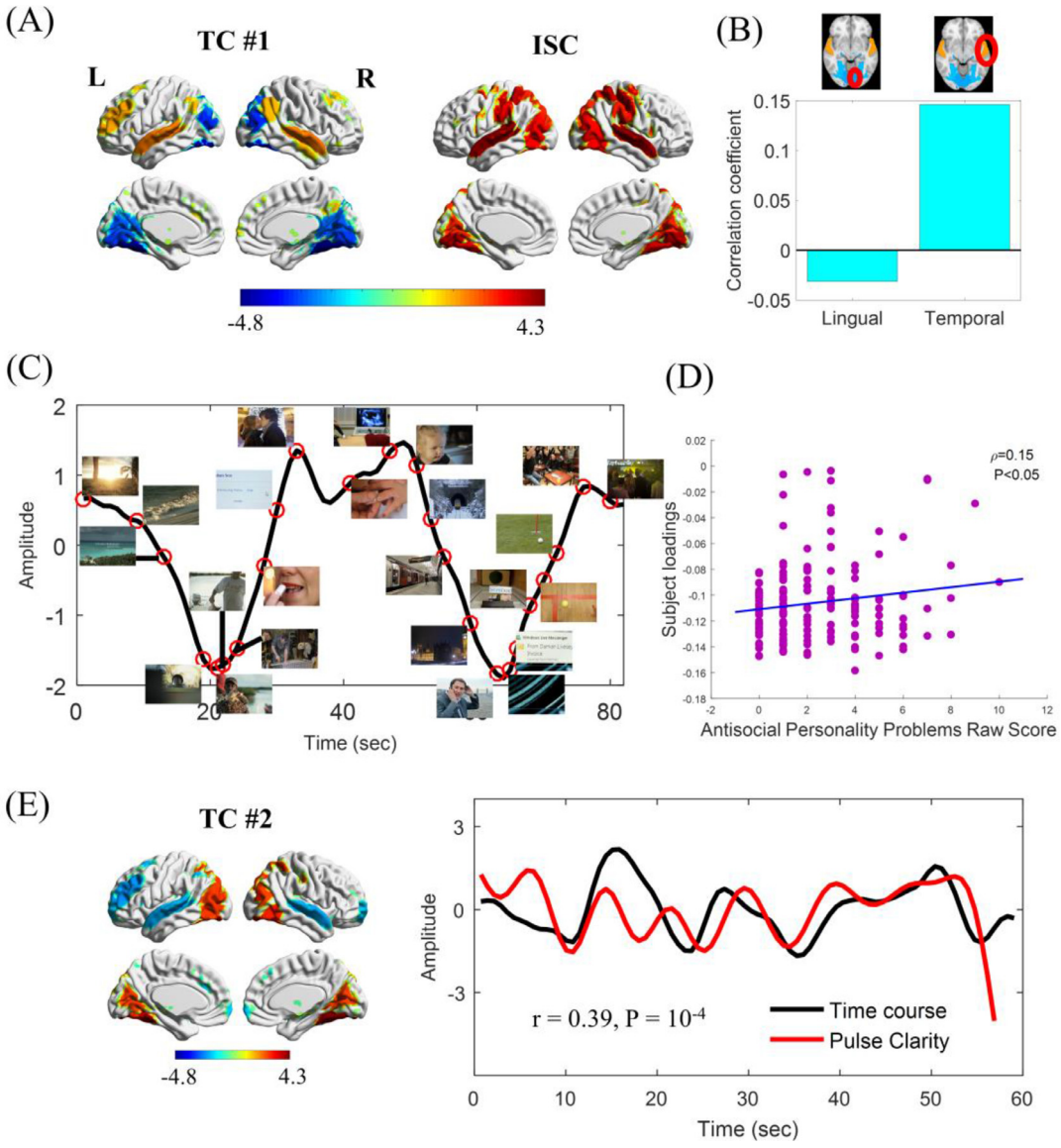

Fig. 5. (A) Spatial maps for the first TCA component, the ISC spatial map. (B) The bar plot shows the average correlation coefficient of subject time courses of lingual gyrus and temporal gyrus with time course estimated with tensor component analysis (TCA). (C) Timeline of the first tensor component with the onset point of each scene. The trends of the timeline with landscape and social related scenes are different. (D) The subject loadings for the first tensor component significantly correlated with Antisocial Personality Problems Raw Score (ρ: correlation coefficient). (E) Spatial map and time course for the second TCA component. The time course of the second tensor component was significantly correlated with the music feature Pulse Clarity ($r = 0.39$, $P = 10^{-4}$).

Supplementary Fig. 4-7) demonstrates that the framework is feasible and capable of extracting interpretable and reproducible components.

Compared with traditional fMRI study designs, naturalistic stimuli are complex and dynamic, and it is much more difficult to generate a model of evoked activity for analyses. With movie stimuli, the time courses of brain activity across subjects are assumed to be consistent across subjects and changing along with ongoing movie scenes. In addition, the brain network(s) that are activated for information processing during movie viewing are assumed to be the same across participants. Based on these assumptions, we have proposed a data-driven TCA framework for characterizing shared spatio-temporal patterns of evoked activity to naturalistic stimuli across subjects. FMRI signals are innately multidimensional and can thus be naturally represented in tensor form. We show that TCA is suitable for naturalistic stimuli fMRI analysis, that our framework is able to estimate in a purely data-driven fashion the brain activity evoked by naturalistic stimuli that corresponds to different stimuli features.

4.1. Merits of TCA framework

The proposed framework has several merits. For naturalistic stimuli fMRI, the variability across subjects has attracted more and more attention (Finn et al., 2020; Nastase et al., 2019), Our proposed framework provides an estimate of subject loadings directly, which can be used to explore individual differences and condition differences. For example, we identified a pattern of evoked activity that had a temporal course related to the presence of social stimuli and loadings that were associated with a measure of antisocial personality problems from a diagnostic interview (Fig. 5 (D)). Even though the relationship between brain network and subjects' traits can also be identified with IS-RSA, the method creates many samples by calculating paired correlation coefficients, which can blur the relationship between brain activity and behavioral measures, resulting in weaker associations. Another merit of our framework is that the brain responses to different features of the naturalistic stimuli can be separated into different patterns (Fig. 4). Third,

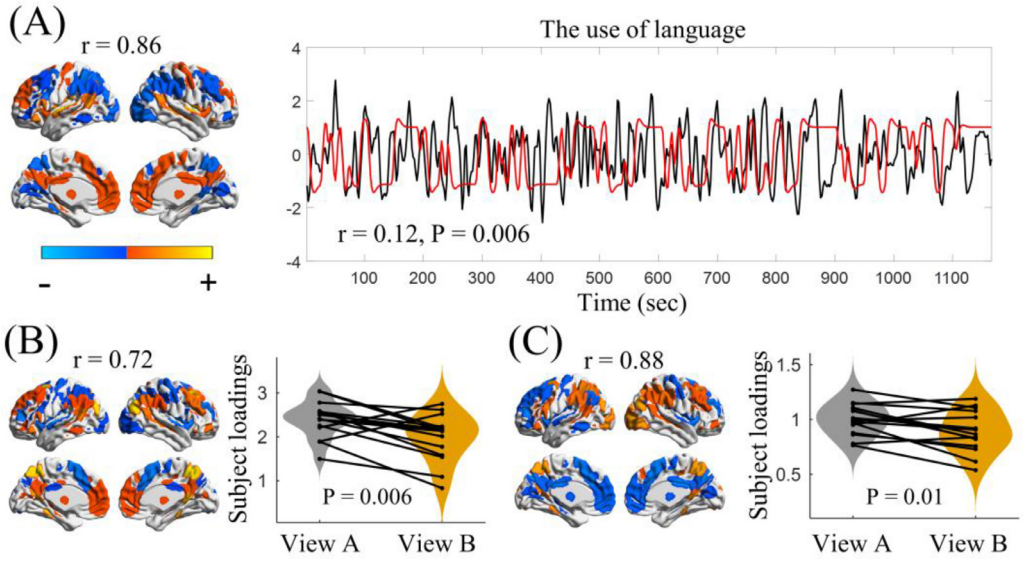

Fig. 6. The estimated tensor components of long-duration movie stimuli. The spatial distributions of these components are highly correlated with spatial distribution estimated with hidden Markov model (HMM). And we also find that the time course of the first tenor component is significantly correlated with the annotation: The use of language (panel A right). Black line represents estimated time courses with TCA. Red line denotes annotation of the use of language convolved with HRF. For both the second and the third tensor components, we found that subject loadings of the second movie viewing (View B) are significantly lower than that of the first movie viewing (View A).

the time courses of the estimated components are estimated without distortion (Fig. 4 & Fig.5(E)), which facilitates the interpretation of the estimated components and represents an advantage over ISFC. Fourth, by combining TCA with evaluation of algorithm stability, the model order is identified in a data-driven manner and reproducibility of the estimation is enhanced (Supplementary, Fig. 3).

In this study, different datasets were used to demonstrate different strengths of the TCA framework applied for naturalistic stimuli fMRI data analysis. Time courses of evoked brain networks can be estimated with both TCA and ISFC. Since the ground truth stimulation time courses are known for traditional task fMRI, motor task fMRI was used to compare the performance of TCA and ISFC in terms of time courses estimation accuracy. The results (Fig. 4) show that TCA captures the time courses of each pattern without destroying temporal attributes, which can happen with ISFC. Preserving the temporal attributes greatly facilitates the interpretation of estimated patterns. HCP movie scenes were used to demonstrate that relativeness of nodes in the same network are better evaluated with TCA framework. In order to demonstrate that TCA framework is also suitable for naturalistic stimuli with longer durations, the van de Meer dataset, previously analyzed with Hidden Markov Modeling, was used. When the TCA framework was applied to the dataset, brain networks with higher occupancy during movie watching than during resting-state were extracted, demonstrating that TCA is suitable for naturalistic stimuli with longer durations and that it is capable of estimating brain activity evoked with naturalistic stimuli that is distinct from spontaneous brain activity.

Improving the reproducibility of neuroscience research is one of greatest concerns for present day neuroimaging research (Poldrack, 2019; Poldrack and Farah, 2015). To guarantee the stability of the TCA algorithm and a suitable model order for the decomposition, a novel spectral clustering algorithm was proposed that is applied to components estimated from multiple runs. In our simulation study, the model order selected based on the proposed algorithm stability index was exactly the same as the number of simulated consistent components across subject, demonstrating that the proposed algorithm stability index identifies an appropriate model order (Fig. 3(A)). In the naturalistic stimuli fMRI study, our results demonstrate that shared spatial-temporal components estimated by our framework are highly reproducible (Supplementary, Fig. 3).

4.2. Comparison with ISC

Both TCA and ISC are based on the assumption that consistent brain activity across subjects occurs when subjects view the same naturalistic stimuli, but the way they estimate the brain activity is different. ISC leverages the correlation across subjects to constrain the spontaneous brain activity and to enhance detection of the brain activity evoked by the naturalistic stimuli. TCA estimates brain activity based on a mathematical model that enables extraction of consistent components across subjects.

Extending ISC to ISFC by combining with a clustering method shows that both ISC and TCA can be used to estimate brain activity that corresponds to different stimulus features, and the spatial distributions of the extracted components are highly consistent across the two methods (Fig. 4). ISC is a relatively simpler approach based on correlations, with extension to ISFC involving the calculation of connectivity matrix across subjects and the addition of k-means clustering. While this approach may be considered more straightforward in terms of implementation and interpretation than TCA analysis, ISFC relies on second-order rather than first-order estimates. This lowers the temporal resolution of the analyses (Fig. 4), which is somewhat limiting in the context of a dynamic stimulus. In particular, this prevents the possibility to pinpoint one particular frame of the movie as driving a given ISFC configuration; rather, any of the data points contributing to the particular estimate may be involved. In the TCA framework, brain temporal activities can be estimated accurately.

Both ISC and TCA can be used to explore subject variability. ISC, via inter-subject representational similarity analysis (Finn et al., 2020; Kriegeskorte et al., 2008; Mantel, 1967; Meer et al., 2020), can be used to explore the relationship between brain activity and behavior at the level of subject pairs. Studies have shown that this method is sensitive to explicit manipulations of attention or prior beliefs about a stimulus (Cooper et al., 2011; Lahnakoski et al., 2014, 2012). Investigation of individual differences using ISC requires the use of non-parametric approaches because the correlations across subjects are highly interdependent, thereby violating the assumption of common parametric tests

(Nastase et al., 2019). In contrast, TCA provides an estimate of subject loadings and the spatial-temporal distribution simultaneously. The subject loadings can then be used to investigate individual variability and condition differences (Fig. 5 & Fig. 6). While this is a strength of TCA, we also found that IS-RSA can identify brain activity related to behavior (Meer et al., 2020) that TCA does not, and as such, these two methods may provide complimentary insights into naturalistic stimuli brain-behavior relationships. For both ISC and TCA, the assumption that different subjects will have the exact same spatial distribution and temporal course in response to naturalistic stimuli may be too strong and may result in difficulty estimating components with slight misalignments across participants, as was found with hand movement in the motor task fMRI study using TCA. Advanced methods that can estimate time-unlocked components are worth exploring in future research.

4.3. Potential data-driven methods for naturalistic stimuli fMRI

Theoretically, some other purely data-driven methods such as spatial ICA (Calhoun et al., 2001; McKeown et al., 1998) and temporal ICA (Smith et al., 2012) can also be applied to naturalistic stimuli fMRI data, although both place constraints in the spatial and temporal domains, respectively, and neither provide subject loadings that can be used to assess inter-subject variability. Spatial ICA assumes that different brain networks are spatially independent and when model order is large enough (>100) (Smith, 2012) the results from this method can be used as brain parcellation, which is the way we used spatial ICA in this paper. Spatial ICA can also be used to separate signal from noise sources and may also identify components that correspond to responses to naturalistic stimuli. However, this method is typically implemented via temporal concatenation of multi-subject data and thus would not necessarily take advantage of similarity in activation responses across subjects. Temporal ICA assumes that statistically independent temporal functional modes exist in the brain, which may not be a realistic assumption considering that some brain networks have correlated or anti-correlated time courses during stimulation. In addition, both of these methods may have difficulty separating spontaneous brain activity from the naturalistic stimulus-evoked brain activity that is immersed within it (Bolton et al., 2018). In our proposed TCA framework, only brain activities that are share spatial-temporal information across subjects are identified, with the spontaneous brain activity being left in the tensor residual, as shown in Fig. 1(C).

4.4. Limitations and future work

There are some limitations to our study. First, we selected a parcellation scheme based on ICA with a particular model order. Several studies (Allen et al., 2014; Jafri et al., 2008; Pervaiz et al., 2020; Smith et al., 2012) have demonstrated that extracted time courses from such parcellations are able to identify intrinsic brain networks when projected into the fMRI data. However, several studies have demonstrated that the model order of the ICA can greatly impact the estimated components (Abou-Elseoud et al., 2010; Beckmann, 2012; Kuang et al., 2018). We recently presented a new algorithm, called Snowball ICA, that estimates components without the need for specifying a model order. This technique relies on extracting the most information from the fMRI data by obviating the impact of the PCA data reduction step associated with specific ICA model orders (Hu et al., 2020). Future work on the TCA framework could be done to investigate the impact of different parcellation schemes.

For motor task fMRI, TCA successfully identify networks evoked by tongue, foot and cues (Fig. 4). However, the algorithm fails to identify a component corresponding to evoked brain activity associated with hand movement. This is because hand movement is sophisticated and the variance across subjects makes it difficult to estimate a common spatio-temporal pattern (Fig. 5) using TCA. Because our algorithm relies on component stability as a criteria for model order selection, the proposed framework will be most suitable to extract those components that have high spatio-temporal consistency across subjects. As shown in the GLM results, the consistency of hand movements across subjects was lower than for other movements (Supplementary Fig. 3), which made it difficult to extract a related component for our implementation of TCA. In this study, the number of extracted tensor components is selected based on the reproducibility of the estimated components. As the number of extracted tensor components increases, the reproducibility of the estimated components is reduced. We also observed that for higher model orders, extracted components generally related to evoked responses in specific participants, rather than reflecting consistent components across subjects. In some contexts, this may not be a limitation. Namely, this could be a strength of our method if one is interested in individual variability, and in the case of hand movements it may be useful for understanding variability that reduced the consistency across subjects. However, more work is needed to determine how best to use these additional components to investigate individual variability.

Naturalistic stimuli fMRI is a powerful tool to study brain network interactions that resemble brain function that occurs as we go about our daily lives. However, care must be taken in identifying suitable naturalistic paradigms. Only three consistent spatial-temporal components were estimated in the movie experiment. Even though the movie's naturalistic stimuli contained plenty of features, variance in the subjects' attention may have reduced the shared evoked responses across subjects. In further studies, the selection or designation of naturalistic stimuli will need to be investigated further to develop stimuli that will result in more consistent stimulus evoked activity.

5. Conclusion

The proposed tensor analysis framework is a powerful method that can extract evoked brain response to naturalistic stimuli that are embedded within resting state brain activity. With the proposed framework, interpretable and reproducible brain states can be extracted and individual variability in the strength of the evoked responses can be assessed. Three types of experiment (simulation, motor task fMRI, naturalistic stimuli fMRI) demonstrated that the proposed framework is a promising tool to extract brain networks evoked with naturalistic stimuli.

Data and Code Availability Statement

The data used in the manuscript are from the human connectome project (HCP; www.humanconnectome.org). The alternating least-squares (ALS) algorithm can be free accessed from tensor toolbox (https://www.tensortoolbox.org). The tensor spectral clustering software is available at https://github.com/GHu-DUT/Tensor_Spectral_Clustering. The analysis code of tensor components analysis framework is available at https://github.com/GHu-DUT/Tensor-components-analysis-for-naturalistic-stimuli-fMRI.

Declaration of Competing Interest

The authors declare that the research was conducted in the absence of any commercial or financial relationships that could be construed as a potential conflict of interest.

Acknowledgments

This work was supported by National Natural Science Foundation of China (Grant No.91748105), National Foundation in China (No. JCKY2019110B009 & 2020-JCJQ-JJ-252) and the Fundamental Research Funds for the Central Universities [DUT2019, DUT20LAB303] in Dalian University of Technology in China. This work was also supported by China Scholarship Council (No.201806060038). LN was supported by the National Institutes of Health (PI: LN, AA024565).

Supplementary materials

Supplementary material associated with this article can be found, in the online version, at doi:10.1016/j.neuroimage.2022.119193.

Appendix: TCA stability analysis with tensor spectral clustering

Background of spectral clustering on graph theory

In this study, a novel tensor spectral clustering algorithm is proposed to evaluate the stability of TCA algorithms. First, we provide some background on spectral clustering. Spectral clustering is a technique with roots in graph theory. Consider an undirected weighted graph G = (V, E), where V is a set of nodes and E is a set of edges reflecting a statistical measure of connectivity between each pair of nodes. The weighted adjacency matrix of G is denoted as a symmetric matrix $\mathbf{W}$. The generalized degree of the nodes in G is defined as $\mathbf{D} = \mathrm{diag}(\mathbf{W}\boldsymbol{e})$, where $\boldsymbol{e}$ is a vector of ones. The combinatorial Laplacian matrix is defined as $\mathbf{K} = \mathbf{D} - \mathbf{W}$. The *transition matrix* of the graph $\mathbf{P} = \mathbf{W}^{\mathrm{T}}\mathbf{D}^{-1}$ is a column stochastic matrix. Thus, the matrix can be interpreted as a Markov chain. The stationary distribution of the Markov chain is given by $\pi = \mathrm{diag}(\mathbf{D})$.

$$\mathbf{P}\mathrm{diag}(\mathbf{D}) = \mathbf{W}^{\mathrm{T}}\mathbf{D}^{-1}\mathrm{diag}(\mathbf{D}) = \mathbf{W}^{\mathrm{T}}\begin{bmatrix} d_1^{-1} & 0 & 0 & 0 \\ 0 & d_2^{-1} & 0 & 0 \\ 0 & 0 & \ddots & 0 \\ 0 & 0 & 0 & d_n^{-1} \end{bmatrix}\begin{bmatrix} d_1 \\ d_2 \\ \vdots \\ d_n \end{bmatrix} = \mathrm{diag}(\mathbf{D}) \tag{A1}$$

In addition, $\mathrm{diag}(\mathbf{D})$ is an eigenvector of $\mathbf{P}$ and the corresponding eigenvalue is one (R.Benson et al., 2015).

In the partition of a graph, it is assumed that the graph can be separated into two parts, S and $\bar{\mathrm{S}}$, then the bottleneck of a graph is defined as the boundary between the two clusters. The bottleneck ratio of any set Ψ is defined as:

$$\Phi(\Psi) = \frac{cut(\mathrm{S})}{\pi(\mathrm{S})}, \tag{A2}$$

where $cut(\mathrm{S}) = \sum_{\mathrm{V}_i \in \mathrm{S},\ \mathrm{V}_j \in \bar{\mathrm{S}}} \mathbf{W}_{ij}$, $\pi(\mathrm{S}) = \sum_{\mathrm{V}_i \in \mathrm{S}} \pi_i$. A small bottleneck ratio indicates a good partition of the graph (Levin et al., 2007).

The indicator vector f over the nodes in G is defined:

$$f_i = \begin{cases} 0 & \mathrm{V}_i \notin \Psi \\ 1 & \mathrm{V}_i \in \Psi \end{cases}. \tag{A3}$$

The property of Laplacian matrix is leveraged as follow:

$$f^{\mathrm{T}}\mathbf{K}f = \frac{1}{2}\sum_{i,j=1}^{n} w_{ij}\left(f_i - f_j\right)^2 = \sum_{\mathrm{V}_i \in \Psi,\ \mathrm{V}_j \in \bar{\Psi}} w_{ij} = cut(\Psi). \tag{A4}$$

Since $\pi = \mathrm{diag}(\mathbf{D})$, $\pi(\Psi)$ could be represented as $f^{\mathrm{T}}\mathbf{D}f$. Hence, the objective of matrix spectral clustering is to find f that minimizes $f^{\mathrm{T}}\mathbf{K}f/f^{\mathrm{T}}\mathbf{D}f$.

Both matrices $\mathbf{K}$ and $\mathbf{D}$ are positive definite. According to generalized Rayleigh entropy, the solution is the vector f such that $\mathbf{K}f = \lambda\mathbf{D}f$. We observed that:

$$\mathbf{K}f = \lambda\mathbf{D}f \Leftrightarrow \left(\mathbf{I} - \mathbf{D}^{-1}\mathbf{W}\right)f = \lambda f \Leftrightarrow \mathbf{P}^{\mathrm{T}}f = (1-\lambda)f \tag{A5}$$

So, the problem is equivalent to computing the eigenvectors of $\mathbf{P}$ (Ng et al., 2002).

Tensor spectral clustering

For multimode tensor spectral clustering (TSC), different modes have different *transition matrices*. In this appendix, a third-order tensor is used as the example for tensor spectral clustering. $\mathbf{P}^{(1)}$, $\mathbf{P}^{(2)}$, $\mathbf{P}^{(3)}$ are three transition matrices for third-order tensor decomposition. They are calculated as follows:

$$\mathbf{P}^{(m)} = \mathbf{W}^{(m)\mathrm{T}}\mathbf{D}^{(m)-1}, \tag{A6}$$

where $\mathbf{D}^{(m)}$ is defined exactly the same as with matrix spectral clustering. The generalized *transition tensor* $\underline{\mathbf{P}}$ can then be defined as:

$$\underline{\mathbf{P}} = \underline{\mathbf{I}} \times_1 \mathbf{P}^{(1)} \times_2 \mathbf{P}^{(2)} \times_3 \mathbf{P}^{(3)}, \tag{A7}$$

where $\underline{\mathbf{I}} \in \mathbb{R}^{RK \times RK \times RK \times RK}$ is a unit tensor, and the number of modes of $\underline{\mathbf{I}}$ are one more than the number of modes of the tensor to be decomposed.

Similar to matrix spectral clustering, generalized singular value decomposition (SVD), Higher-order singular value decomposition (HOSVD, Lieven et al., 2000), is applied to the *transition tensor* $\underline{\mathbf{P}}$. For HOSVD of $\underline{\mathbf{P}}$, the essence of the decomposition of the last mode is the eigenvalue decomposition of the covariance matrix for the matrix unfolding of tensor $\underline{\mathbf{P}}$ on the last mode. The unfolding of tensor $\underline{\mathbf{P}}$ on the last mode is denoted as $\underline{\mathbf{P}}_{(\mathrm{end})}$, which is calculated as follow:

$$\underline{\mathbf{P}}_{(\mathrm{end})} = \underline{\mathbf{I}}_{(\mathrm{end})}\left(\mathbf{P}^{(1)} \otimes \mathbf{P}^{(2)} \otimes \mathbf{P}^{(2)}\right)^{\mathrm{T}}. \tag{A8}$$

The covariance matrix of $\underline{\mathbf{P}}_{(\mathrm{end})}$ is:

$$\underline{\mathbf{P}}_{(\mathrm{end})}\underline{\mathbf{P}}_{(\mathrm{end})}{}^{\mathrm{T}} = \underline{\mathbf{I}}_{(\mathrm{end})}\left(\mathbf{P}^{(1)} \otimes \mathbf{P}^{(2)} \otimes \mathbf{P}^{(3)}\right)^{\mathrm{T}}\left(\underline{\mathbf{I}}_{(\mathrm{end})}\left(\mathbf{P}^{(1)} \otimes \mathbf{P}^{(2)} \otimes \mathbf{P}^{(3)}\right)^{\mathrm{T}}\right)^{\mathrm{T}}. \tag{A9}$$

We defined the following:

$$\mathbf{W}_{\mathrm{TSC}} = \mathbf{W}^{(1)}\mathbf{W}^{(1)} \circledast \mathbf{W}^{(2)}\mathbf{W}^{(2)} \circledast \mathbf{W}^{(3)}\mathbf{W}^{(3)} \tag{A10}$$

$$\mathbf{D}_{\mathrm{TSC}} = \mathbf{D}^{(1)}\mathbf{D}^{(1)} \circledast \mathbf{D}^{(2)}\mathbf{D}^{(2)} \circledast \mathbf{D}^{(3)}\mathbf{D}^{(3)} \tag{A11}$$

$$\mathbf{K}_{\mathrm{TSC}} = \mathbf{D}_{\mathrm{TSC}} - \mathbf{W}_{\mathrm{TSC}} \tag{A12}$$

$\mathbf{W}_{\mathrm{TSC}}$ is a symmetric matrix and represents weighted adjacency matrix of TSC. $\mathbf{D}_{\mathrm{TSC}}$ is a diagonal matrix. Both matrices $\mathbf{K}_{\mathrm{TSC}}$ and $\mathbf{D}_{\mathrm{TSC}}$ are positive definite. Then equation (A9) can be reduced as follows:

$$\mathbf{P}_{\mathrm{TSC}} = \mathbf{D}_{\mathrm{TSC}}^{-1/2}\mathbf{W}_{\mathrm{TSC}}\mathbf{D}_{\mathrm{TSC}}^{-1/2} = \underline{\mathbf{P}}_{(\mathrm{end})}\underline{\mathbf{P}}_{(\mathrm{end})}{}^{\mathrm{T}}. \tag{A13}$$

Similar to matrix spectral clustering, the purpose of tensor spectral clustering is to find f that minimizes $f^{\mathrm{T}}\mathbf{K}_{\mathrm{TSC}}f/f^{\mathrm{T}}\mathbf{D}_{\mathrm{TSC}}f$. Based on the generalized Rayleigh entropy and diagonal property of $\mathbf{D}_{\mathrm{TSC}}$, the objective function:

$$f^{\mathrm{T}}\mathbf{K}_{\mathrm{TSC}}f/f^{\mathrm{T}}\mathbf{D}_{\mathrm{TSC}}f = f^{\mathrm{T}}\left(\mathbf{D}_{\mathrm{TSC}} - \mathbf{W}_{\mathrm{TSC}}\right)f/f^{\mathrm{T}}\mathbf{D}_{\mathrm{TSC}}f \tag{A14}$$

is equivalent to finding f to minimize $f^{\mathrm{T}}\left(\mathbf{I} - \mathbf{D}_{\mathrm{TSC}}^{-1/2}\mathbf{W}_{\mathrm{TSC}}\mathbf{D}_{\mathrm{TSC}}^{-1/2}\right)f = f^{\mathrm{T}}\left(\mathbf{I} - \mathbf{P}_{\mathrm{TSC}}\right)f$.

At this stage, the problem of tensor spectral clustering is reduced to matrix spectral clustering. So, the last mode eigenvector of HOSVD of the *transition tensor* $\underline{\mathbf{P}}$ can be used for multimode co-clustering.

Given a set of samples that we want to cluster into k subsets, and each sample has more than one modality to be considered, the procedure of TSC is as follows:

1. Form the weighted adjacency matrices of each modality: $\mathbf{W}^{(1)}$, $\mathbf{W}^{(2)}$, $\mathbf{W}^{(3)}$,….
2. Define the *transition matrix* of each modality: $\mathbf{P}^{(1)}$, $\mathbf{P}^{(2)}$, $\mathbf{P}^{(2)}$, …. Then the *transition tensor* $\underline{\mathbf{P}}$ is defined with equation (A7).
3. Find the k eigenvectors $\boldsymbol{v}_1, \boldsymbol{v}_2, \cdots, \boldsymbol{v}_k$ corresponding to the k largest eigenvalues of the last mode of *transition tensor* $\underline{\mathbf{P}}$ with HOSVD. Form the matrix $\mathbf{V} = [\ \boldsymbol{v}_1, \boldsymbol{v}_2, \cdots, \boldsymbol{v}_k\ ]$ by concatenating eigenvectors in columns.
4. Normalize each row of $\mathbf{V}$ to have unit length $\mathbf{L}_{i,j} = \mathbf{V}_{i,j}/(\sum_j \mathbf{V}_{i,\,j}^2)^{1/2}$.
5. Cluster points, each row of $\mathbf{L}$, into k clusters via Hierarchical clustering (Gordon, 1987).
6. Find the corresponding row i of $\mathbf{L}$ and original sample, assign the original sample to the cluster j that row i assigned.

Software for tensor spectral clustering is available at https://github.com/GHu-DUT/Tensor_Spectral_Clustering.

For the stability analysis of TCA algorithms, for the given dataset, the same algorithm with the same parameters is ran K times. Given

the number of extracted components R, for each mode, there are $R \times K$ components. When TSC is applied during the stability analysis of TCA, the similarity matrices of each mode $\mathbf{W}^{(\mathbf{S})}$, $\mathbf{W}^{(\sigma)}$, $\mathbf{W}^{(\mathbf{C})}$ work as weighted adjacency matrices. Furthermore, eigenvectors of last mode of the *transition tensor* $\underline{\mathbf{P}}$ are fed into Hierarchical clustering. The number of clusters is defined as exactly same as the number of extracted components R, with stable components producing a tight cluster. The stability index is quantified with the average intra-cluster similarities

$$I_s(S_k) = \frac{1}{N} \sum_{i,j \in S_k} \langle \mathbf{L}_i, \mathbf{L}_j \rangle, \tag{A15}$$

where S_k is the set of indices that belong to the kth cluster and $\langle \mathbf{L}_i, \mathbf{L}_j \rangle$ represents similarity between ith and jth components. Ideally, if the extraction of the component is stable, the inner similarity of the corresponding cluster is close to 1 and the stability index of unstable components approaches 0. The algorithm stability is defined as the average of components stability indices. When the selected model order is appropriate for the tensor being decomposed, the algorithm will be stable. Hence, hyperparameters such as the model order can be selected in terms of algorithm stability.

References

Abou-Elseoud, A., Starck, T., Remes, J., Nikkinen, J., Tervonen, O., Kiviniemi, V., 2010. The effect of model order selection in group PICA. Hum. Brain Mapp. 31, 1207–1216. doi:10.1002/hbm.20929.

Akaike, H., 1998. Information theory and an extension of the maxi-mum likelihood principle. Sel. Pap. hirotugu akaike 199–213.

Allen, E.A., Damaraju, E., Plis, S.M., Erhardt, E.B., Eichele, T., Calhoun, V.D., 2014. Tracking whole-brain connectivity dynamics in the resting state. Cereb. Cortex 24, 663–676. doi:10.1093/cercor/bhs352.

Alluri, V., Toiviainen, P., Jääskeläinen, I.P., Glerean, E., Sams, M., Brattico, E., 2012. Large-scale brain networks emerge from dynamic processing of musical timbre, key and rhythm. Neuroimage 59, 3677–3689. doi:10.1016/j.neuroimage.2011.11.019.

Andersen, A.H., Rayens, W.S., 2004. Structure-seeking multilinear methods for the analysis of fMRI data. Neuroimage 22, 728–739. doi:10.1016/j.neuroimage.2004.02.026.

Baldassano, X.C., Hasson, X.U., Norman, X.K.A., 2018. Representation of Real-World Event Schemas during Narrative Perception. J. Neurosci. 38, 9689–9699.

Barch, D.M., Burgess, G.C., Harms, M.P., Petersen, S.E., Schlaggar, B.L., Corbetta, M., Glasser, M.F., Curtiss, S., Dixit, S., Feldt, C., Nolan, D., Bryant, E., Hartley, T., Footer, O., Bjork, J.M., Poldrack, R., Smith, S., Johansen-Berg, H., Snyder, A.Z., Essen, D.C.Van, 2013. Function in the human connectome: Task-fMRI and individual differences in behavior. Neuroimage 80, 169–189. doi:10.1016/j.neuroimage.2013.05.033.

Beckmann, C.F., 2012. Modelling with independent components. Neuroimage 62, 891–901. doi:10.1016/j.neuroimage.2012.02.020.

Beckmann, C.F., Smith, S.M., 2005. Tensorial extensions of independent component analysis for multisubject FMRI analysis. Neuroimage 25, 294–311. doi:10.1016/j.neuroimage.2004.10.043.

Bolton, T.A.W., Ville, D.Van De, Giraud, D.J.A., 2018. Brain dynamics in ASD during movie-watching show idiosyncratic functional integration and segregation. Hum. Brain Mapp 2391–2404. doi:10.1002/hbm.24009.

Bucholz, K.K., Cadoret, R., Cloninger, C.R., Dinwiddie, S.H., Hesselbrock, V.M., Nurnberger, J.I., Reich, T., Schmidt, I., Schuckit, M.A., 1994. A new, semi-structured psychiatric interview for use in genetic linkage studies: A report on the reliability of the SSAGA. J. Stud. Alcohol 55, 149–158. doi:10.15288/jsa.1994.55.149.

Calhoun, V.D., Adali, T., Pearlson, G.D., Pekar, J.J., 2001. A method for making group inferences from functional mri data using independent component analysis. hum. Brain Mapp 14, 96–107. doi:10.1002/hbm.

Chen, J., Honey, C.J., Simony, E., Arcaro, M.J., Norman, K.A., Hasson, U., 2016. Accessing real-life episodic information from minutes versus hours earlier modulates hippocampal and high-order cortical dynamics. Cereb. Cortex 26, 3428–3441. doi:10.1093/cercor/bhv155.

Chen, J., Leong, Y.C., Honey, C.J., Yong, C.H., Norman, K.A., Hasson, U., 2017. Shared memories reveal shared structure in neural activity across individuals. Nat. Neurosci. 20, 115–125. doi:10.1038/nn.4450.

Cichocki, A., Mandic, D., De Lathauwer, L., Zhou, G., Zhao, Q., Caiafa, C., Phan, H.A., 2015. Tensor decompositions for signal processing applications: From two-way to multiway component analysis. IEEE Signal Process. Mag. 32, 145–163. doi:10.1109/MSP.2013.2297439.

Cong, F., He, Z., Hamalainen, J., Cichocki, A., Ristaniemi, T., 2011. Determining the number of sources in high-density eeg recordings of event-related potentials by model order selection. In: IEEE International Workshop on Machine Learning for Signal Processing, pp. 1–6.

Cong, F., Lin, Q.-H., Kuang, L.-D., Gong, X.-F., Astikainen, P., Ristaniemi, T., 2015a. Tensor decomposition of EEG signals: a brief review. J. Neurosci. Methods 248, 59–69. doi:10.1016/j.jneumeth.2015.03.018.

Cong, F., Ristaniemi, T., Lyytinen, H., 2015b. Advanced signal processing on eventrelated potentials (ERPs). https://doi.org/10.1142/9789814623094

Cooper, E.A., Hasson, U., Small, S.L., 2011. Interpretation-mediated changes in neural activity during language comprehension. Neuroimage 55, 1314–1323. doi:10.1016/j.neuroimage.2011.01.003.

Eickhoff, S.B., Milham, M., Vanderwal, T., 2020. Towards clinical applications of movie fMRI. Neuroimage 217, 116860. doi:10.1016/j.neuroimage.2020.116860.

Erhardt, E.B., A.Allen, E., Wei, Y., Eichele, T., D.Calhoun, V., 2012. SimTB, a simulation toolbox for fMRI data under a model of spatiotemporal separability. Neuroimage 59, 4160–4167. doi:10.1016/j.dcn.2011.01.002.

Esteban, O., Markiewicz, C.J., Blair, R.W., Moodie, C.A., Isik, A.I., Erramuzpe, A., Kent, J.D., Goncalves, M., DuPre, E., Snyder, M., Oya, H., Ghosh, S.S., Wright, J., Durnez, J., Poldrack, R.A., Gorgolewski, K.J., 2019. fMRIPrep: a robust preprocessing pipeline for functional MRI. Nat. Methods 16, 111–116. doi:10.1038/s41592-018-0235-4.

Finn, E.S., Glerean, E., Khojandi, A.Y., Nielson, D., Molfese, P.J., Handwerker, D.A., Bandettini, P.A., 2020. Idiosynchrony: From shared responses to individual differences during naturalistic neuroimaging. Neuroimage 215, 116828. doi:10.1016/j.neuroimage.2020.116828.

Garrison, K.A., Scheinost, D., Finn, E.S., Shen, X., Constable, R.T., 2015. The (in)stability of functional brain network measures across thresholds. Neuroimage 118, 651–661. doi:10.1016/j.neuroimage.2015.05.046.

Glasser, M.F., Coalson, T.S., Robinson, E.C., Hacker, C.D., Harwell, J., Yacoub, E., Ugurbil, K., Andersson, J., Beckmann, C.F., Jenkinson, M., Smith, S.M., Van Essen, D.C., 2016. A multi-modal parcellation of human cerebral cortex. Nature 536, 171–178. doi:10.1038/nature18933.

Glasser, M.F., Sotiropoulos, S.N., Wilson, J.A., Coalson, T.S., Fischl, B., Andersson, J.L., Xu, J., Jbabdi, S., Webster, M., Polimeni, J.R., Van Essen, D.C., Jenkinson, M., 2013. The minimal preprocessing pipelines for the Human Connectome Project. Neuroimage 80, 105–124. doi:10.1016/j.neuroimage.2013.04.127.

Gordon, A., 1987. A Review of Hierarchical Classification. J. R. Stat. Soc. Ser. A 150, 119–137.

Griffanti, L., Salimi-Khorshidi, G., Beckmann, C.F., Auerbach, E.J., Douaud, G., Sexton, C.E., Zsoldos, E., Ebmeier, K.P., Filippini, N., Mackay, C.E., Moeller, S., Xu, J., Yacoub, E., Baselli, G., Ugurbil, K., Miller, K.L., Smith, S.M., 2014. ICA-based artefact removal and accelerated fMRI acquisition for improved resting state network imaging. Neuroimage 95, 232–247. doi:10.1016/j.neuroimage.2014.03.034.

Hasson, U., Nir, Y., Levy, I., Fuhrmann, G., Malach, R., 2004. Intersubject Synchronization of Cortical Activity During Natural Vision. Science 303 (80-), 1634–1640. doi:10.1126/science.1089506.

Haxby, J.V., Connolly, A.C., Guntupalli, J.S., 2014. Decoding neural representational spaces using multivariate pattern analysis. Annu. Rev. Neurosci. 37, 435–456. doi:10.1146/annurev-neuro-062012-170325.

Helwig, N.E., Hong, S., 2013. A critique of tensor probabilistic independent component analysis: implications and recommendations for multi-subject fMRI data analysis. J. Neurosci. Methods 213, 263–273. doi:10.1016/j.jneumeth.2012.12.009.

Hesselbrock, M., Easton, C., Kathleen, K., Schuckit, M., Hesselbrock, V., 1999. A validity study of the SSAGA a comparison with the SCAN. Addiction 94, 1361–1370.

Hitchcock, F.L., 1927. The expression of a tensor or a polyadic as a sum of products. J. Math. Phys. 6, 164–189. doi:10.1002/sapm192761164.

Hu, G., Wang, D., Luo, S., Hao, Y., Nickerson, L.D., Cong, F., 2021. Frequency specific co-activation pattern analysis via sparse nonnegative tensor decomposition. J. Neurosci. Methods 362, 109299. doi:10.1016/j.jneumeth.2021.109299.

Hu, G., Waters, A.B., Aslan, S., Frederick, B., Cong, F., Nickerson, D.L., 2020. Snowball ICA : a model order free independent component analysis strategy for functional magnetic resonance imaging data. Front. Neurosci. 14, 1–15. doi:10.3389/fnins.2020.569657.

Huth, A.G., Heer, W.A.De, Griffiths, T.L., Theunissen, F.E., Jack, L., 2016. Natural speech reveals the semantic maps that tile human cerebral cortex. Nature 532, 453–458. doi:10.1038/nature17637.

Jafri, M.J., Pearlson, G.D., Stevens, M., Calhoun, V.D., 2008. A method for functional network connectivity among spatially independent resting-state components in schizophrenia. Neuroimage 39, 1666–1681. doi:10.1016/j.neuroimage.2007.11.001.

Kauppi, J.P., Pajula, J., Tohka, J., 2014. A versatile software package for inter-subject correlation based analyses of fMRI. Front. Neuroinform. 8, 1–13. doi:10.3389/fninf.2014.00002.

Kolda, T.G., Bader, B.W., 2009. Tensor decompositions and applications. SIAM Rev 51, 455–500. doi:10.1137/07070111X.

Kriegeskorte, N., Mur, M., Bandettini, P., 2008. Representational similarity analysis – connecting the branches of systems neuroscience. Front. Syst. Neurosci. 2, 1–28. doi:10.3389/neuro.06.004.2008.

Kuang, L.D., Lin, Q.H., Gong, X.F., Cong, F., Sui, J., Calhoun, V.D., 2018. Model order effects on ICA of resting-state complex-valued fMRI data: application to schizophrenia. J. Neurosci. Methods 304, 24–38. doi:10.1016/j.jneumeth.2018.02.013.

Kuang, L.D., Lin, Q.H., Gong, X.F., Cong, F., Sui, J., Calhoun, V.D., 2015. Multi-subject fMRI analysis via combined independent component analysis and shift-invariant canonical polyadic decomposition. J. Neurosci. Methods 256, 127–140. doi:10.1016/j.jneumeth.2015.08.023.

Kuang, L.D., Lin, Q.H., Gong, X.F., Cong, F., Wang, Y.P., Calhoun, V.D., 2020. Shift-Invariant Canonical Polyadic Decomposition of Complex-Valued Multi-Subject fMRI Data with a Phase Sparsity Constraint. IEEE Trans. Med. Imaging 39, 844–853. doi:10.1109/TMI.2019.2936046.

Lahnakoski, J.M., Glerean, E., Jääskeläinen, I.P., Hyönä, J., Hari, R., Sams, M., Nummenmaa, L., 2014. Synchronous brain activity across individuals underlies shared psychological perspectives. Neuroimage 100, 316–324. doi:10.1016/j.neuroimage.2014.06.022.

Lahnakoski, J.M., Salmi, J., Jääskeläinen, I.P., Lampinen, J., Glerean, E., Tikka, P., Sams, M., 2012. Stimulus-related independent component and voxel-wise analy-

sis of human brain activity during free viewing of a feature film. PLoS One 7. doi:10.1371/journal.pone.0035215.
Lartillot, O.T., 2007. MIR in Matlab (II): a toolbox for musical feature extraction from audio. Dixon, S., Bainbridge, D., Typke, Rainer (Eds.). In: Proc. Intl. Conf. Music Inform., pp. 237–244.
Lerner, Y., Honey, C.J., Silbert, L.J., Hasson, U., 2011. Topographic mapping of a hierarchy of temporal receptive windows using a narrated story. J. Neurosci. 31, 2906–2915. doi:10.1523/JNEUROSCI.3684-10.2011.
Levin, D.A., Peres, Y., Wilmer, E.L., Propp, J., Wilson, D.B., 2007. Markov chains and mixing times. American Mathematical Soc.
Lieven, D.L., Bart, D.M., Joos, V., 2000. A multilinear singular value decomposition. SIAM J. Matrix Anal. Appl. 21, 1253–1278.
Mantel, N., 1967. The detection of disease clustering and a generalized regression approach. Cancer Res. 27, 209–220.
McKeown, M.J., Makeig, S., Brown, G.G., Jung, T.-P., Kindermann, S.S., Bell, a J., Sejnowski, T.J., 1998. Analysis of fMRI data by blind separation into independent components. Hum. Brain Mapp. 6, 160–188.
Meer, J.N., va. der, Breakspear, M., Chang, L.J., Sonkusare, S., Cocchi, L., 2020. Movie viewing elicits rich and reliable brain state dynamics. Nat. Commun. 11, 1–14. doi:10.1038/s41467-020-18717-w.
Mørup, M., Hansen, L.K., Arnfred, S.M., Lim, L.H., Madsen, K.H., 2008. Shift-invariant multilinear decomposition of neuroimaging data. Neuroimage 42, 1439–1450. doi:10.1016/j.neuroimage.2008.05.062.
Nastase, S.A., Gazzola, V., Hasson, U., Keysers, C., 2019. Measuring shared responses across subjects using intersubject correlation. Soc. Cogn. Affect. Neurosci. 14, 669–687. doi:10.1093/scan/nsz037.
Ng, A.Y., Jordan, M.I., Weiss, Y., 2002. On spectral clustering: analysis and an algorithm. Adv. Neural Inf. Process. Syst. 849–856 https://doi.org/10.1.1.19.8100.
Nickerson, L.D., Smith, S.M., Öngür, D., Beckmann, C.F., 2017. Using dual regression to investigate network shape and amplitude in functional connectivity analyses. Front. Neurosci. 11, 115. doi:10.3389/fnins.2017.00115.
Nishimoto, S., Vu, A.T., Naselaris, T., Benjamini, Y., Yu, B., Gallant, J.L., 2011. Reconstructing visual experiences from brain activity evoked by natural movies. Curr. Biol. 21, 1641–1646. doi:10.1016/j.cub.2011.08.031.Reconstructing.
Norman, K.A., Polyn, S.M., Detre, G.J., Haxby, J.V., 2006. Beyond mind-reading: multi-voxel pattern analysis of fMRI data. Trends Cogn. Sci. 10, 424–430. doi:10.1016/j.tics.2006.07.005.
Pervaiz, U., Vidaurre, D., Woolrich, M.W., Smith, S.M., 2020. Optimising network modelling methods for fMRI. Neuroimage 211, 116604. doi:10.1016/j.neuroimage.2020.116604.
Poldrack, R.A., 2019. The Costs of Reproducibility. Neuron 101, 11–14. doi:10.1016/j.neuron.2018.11.030.
Poldrack, R.A., Farah, M.J., 2015. Progress and challenges in probing the human brain. Nature 526, 371–379.
R.Benson, A., F.Gleich, D., Leskovec, J., 2015. Tensor spectral clustering for partitioning higher-order network structures. In: Proc. 2015 SIAM Int. Conf. Data Min, pp. 118–126. doi:10.1016/j.chemosphere.2012.12.037.Reactivity.
Rissanen, J., 1978. Modelling by the shortest data description. Automatica 14, 465–471.
Salimi-Khorshidi, G., Douaud, G., Beckmann, C.F., Glasser, M.F., Griffanti, L., Smith, S.M., 2014. Automatic denoising of functional MRI data: combining independent component analysis and hierarchical fusion of classifiers. Neuroimage 90, 449–468. doi:10.1016/j.neuroimage.2013.11.046.
Shirer, W.R., Ryali, S., Rykhlevskaia, E., Menon, V., Greicius, M.D., 2012. Decoding subject-driven cognitive states with whole-brain connectivity patterns. Cereb. Cortex 22, 158–165. doi:10.1093/cercor/bhr099.
Simony, E., Chang, C., 2020. Analysis of stimulus-induced brain dynamics during naturalistic paradigms. Neuroimage 216, 116461. doi:10.1016/j.neuroimage.2019.116461.
Simony, E., Honey, C.J., Chen, J., Lositsky, O., Yeshurun, Y., Wiesel, A., Hasson, U., 2016. Dynamic reconfiguration of the default mode network during narrative comprehension. Nat. Commun. 7. doi:10.1038/ncomms12141.
Smith, S.M., 2012. The future of FMRI connectivity. Neuroimage 62, 1257–1266. doi:10.1016/j.neuroimage.2012.01.022.
Smith, S.M., Feinberg, D.A., Moeller, S., Yacoub, E.S., Auerbach, E.J., Woolrich, M.W., Glasser, M.F., Van Essen, D.C., Xu, J., Jenkinson, M., Andersson, J., Miller, K.L., Beckmann, C.F., Ugurbil, K., 2012. Temporally-independent functional modes of spontaneous brain activity. Proc. Natl. Acad. Sci. 109, 3131–3136. doi:10.1073/pnas.1121329109.
Sonkusare, S., Breakspear, M., Guo, C., 2019. Naturalistic stimuli in neuroscience: critically acclaimed. Trends Cogn. Sci. 23, 699–714. doi:10.1016/j.tics.2019.05.004.
Spiers, H.J., Maguire, E.A., 2007. Decoding human brain activity during real-world experiences. Trends Cogn. Sci. 11, 356–365. doi:10.1016/j.tics.2007.06.002.
Vu, T., Jamison, A., Glasser, K., Simith, M.F., Coalson, S.M., Moeller, T., Auerbach, S., Uğurbil, E.J., Yacoub, K., 2016. Tradeoffs in pushing the spatial resolution of fMRI for the 7T human connectome project. Neuroimage 154, 23–32. doi:10.1016/j.neuroimage.2016.11.049.
Van Essen, D.C., Smith, S.M., Barch, D.M., Behrens, T.E.J., Yacoub, E., Ugurbil, K., Consortium, W.-M.H., 2013. The WU-Minn human connectome project: an overview. Neuroimage 80, 62–79. doi:10.1016/j.neuroimage.2013.05.041.
Van Essen, D.C., Ugurbil, K., Auerbach, E., Barch, D., Behrens, T.E.J., Bucholz, R., Chang, A., Chen, L., Corbetta, M., Curtiss, S.W., Della Penna, S., Feinberg, D., Glasser, M.F., Harel, N., Heath, A.C., Larson-Prior, L., Marcus, D., Michalareas, G., Moeller, S., Oostenveld, R., Petersen, S.E., Prior, F., Schlaggar, B.L., Smith, S.M., Snyder, A.Z., Xu, J., Yacoub, E., 2012. The human connectome project: a data acquisition perspective. Neuroimage 62, 2222–2231. doi:10.1016/j.neuroimage.2012.02.018.
Wang, D., Zhu, Y., Ristaniemi, T., Cong, F., 2018. Extracting multi-mode ERP features using fifth-order nonnegative tensor decomposition. J. Neurosci. Methods 308, 240–247. doi:10.1016/j.jneumeth.2018.07.020.
Williams, A.H., Kim, T.H., Wang, F., Vyas, S., Ryu, S.I., Shenoy, K.V., Schnitzer, M., Kolda, T.G., Ganguli, S., 2018. Unsupervised discovery of demixed, low-dimensional neural dynamics across multiple timescales through tensor component analysis. Neuron 98, 1099–1115. doi:10.1016/j.neuron.2018.05.015.
Wolf, I., Dziobek, I., Heekeren, H.R., 2010. Neural correlates of social cognition in naturalistic settings: A model-free analysis approach. Neuroimage 49, 894–904. doi:10.1016/j.neuroimage.2009.08.060.
Zhou, G., Cichocki, A., 2012. Canonical polyadic decomposition based on a single mode blind source separation. IEEE Signal Process. Lett. 19, 523–526.
Zhou, G., Cichocki, A., Zhao, Q., Xie, S., 2014. Nonnegative matrix and tensor factorizations: an algorithmic perspective. IEEE Signal Process. Mag. 31, 54–65. doi:10.1109/MSP.2014.2298891.
Zhu, Y., Liu, J., Ye, C., Mathiak, K., Astikainen, P., Ristaniemi, T., Cong, F., 2020a. Discovering dynamic task-modulated functional networks with specific spectral modes using MEG. Neuroimage 218, 116924. doi:10.1016/j.neuroimage.2020.116924.
Zhu, Y., Member, S., Liu, J., Member, S., Mathiak, K., 2020b. Deriving electrophysiological brain network connectivity via tensor component analysis during freely listening to music. IEEE Trans. Neural Syst. Rehabil. Eng. 28, 409–418. doi:10.1109/TNSRE.2019.2953971.